doi: 10.2166/9781789062977_0421

Chapter 19

CFD as a Tool for Modelling Membrane Systems

Gustavo A. Fimbres Weihs, The University of Sydney, Australia

Francisco Javier García Picazo, City of San Diego, USA

Yie Kai Chong, Wen Yew Lam, Jia Xin Tan, Kathleen Foo,

Weng Fung Twong, Yong Yeow Liang,

Universiti Malaysia Pahang Al-Sultan Abdullah, Malaysia

The learning objectives of this chapter are the following:

- Define basic principles of CFD
- Define and apply CFD for modelling membrane systems
- Present and discuss the equations involved and steps for building a CFD model of a membrane system
- Understand the theoretical background of mass transport and permeate flux and how they interplay to result in concentration polarisation and fouling.

19.1 INTRODUCTION

Computational fluid dynamics (CFD) is a computer-based numerical method used to analyse systems that involve fluid flow and/or heat and mass transfer (Versteeg & Malalasekera, 2007). CFD bridges the two different approaches for solving engineering problems before the computer era, theoretical and experimental; it relies on mathematical models while being easy to adapt to almost any realistic condition (Anderson & Wendt, 1995). Another feature of CFD is its versatility, as it allows the analysis of systems for a variety of applications such as chemical reactions (Salehi *et al.*, 2016), aerodynamics (Snel, 2003), dispersion of pollutants (Chu *et al.*, 2005), blood flows (Byun & Rhee, 2004), among many others.

The popularity of CFD has increased as the processing power of computers has become more capable in the last decades. Some of the advantages of CFD over experiment-based approaches for analysing and understanding systems are (Versteeg & Malalasekera, 2007):

- significantly higher resolution,
- excellent reproducibility and repeatability,
- ability to analyse complex systems,
- capacity to extract multiple characteristics of the fluid (velocity, concentration, vorticity, etc.),
- non-intrusiveness, and
- set-up cost and time reduction.

Theoretical analysis of fluids is typically intractable for realistic conditions, so typically several assumptions are considered in order to be able to solve these models (Wiley & Fletcher, 2003). In addition, these simplified analytical models are very difficult to validate in the laboratory due to the presence of external sources of noise (Liang *et al.*, 2020b). In those cases, CFD stands out a useful technique as it allows the study of complex models that are difficult to analyse mathematically or to set up experimentally, albeit at the expense of computational power.

There are multiple software options available to perform CFD analysis, including commercial offerings such as ANSYS-Fluent®, ANSYS-CFX® and COMSOL-Multiphysics®, as well as freely available open-source options such as OpenCFD-OpenFOAM® (Table 1). The most general differences between them are the user interface, the flexibility to edit the simulation parameters and the numerical approach used to obtain the results. In general, they all make use of the computer CPU (ANSYS-CFX®) to perform calculations, while some may use the GPU or both (ANSYS-Fluent®). The selection of software should be based on the type of analysis being performed.

Table 1 Commercially available software for CFD analysis and their characteristics

Software	Developer	Type	Method	Reference	Used by
Fluent®	ANSYS	Proprietary	Cell-centred finite volume or finite element	ANSYS Inc. (2020)	Gavelli *et al.* (2008), Liu *et al.* (2013), Su *et al.* (2019)
CFX®	ANSYS	Proprietary	Cell-vertex finite volume	ANSYS Inc. (2012)	Liang *et al.* (2018b), Toh *et al.* (2020b)
Multiphysics®	COMSOL	Proprietary	Finite element	COMSOL AB (2008)	Baghel *et al.* (2020), Brunner *et al.* (2018)
OpenFOAM®	OpenCFD	Open source	Cell-centred finite volume	OpenCFD Ltd. (2016)	Haddadi *et al.* (2018), Liu and Hinrichsen (2014), Kone *et al.* (2018)

19.1.1 What is NOT modelled

As any other analysis method, CFD presents some limitations that are worthy of note when considering it for the analysis of fluid flows. For instance, some simulations may require very large computational time to perform even using specialised hardware. The use of high-performance computing hardware can significantly reduce the computational time, but this is often expensive (Jamshed, 2015). In addition, CFD is not suitable for all cases or purposes; for example, simulation of the transport of individual molecules in a fluid domain can be extremely difficult (or even impossible) to model. Determining the effect of the physicochemical properties of a membrane on its transport performance is also not within the applications of CFD, as the relevant phenomena do not occur in the fluid phase but within the membrane matrix. Moreover, CFD is not useful to determine the effect of the membrane roughness on the boundary layer, as roughness is in order of 10 nm (Boussu *et al.*, 2005), while the concentration boundary layer typically ranges from 1 to 100 μm in thickness (Rodrigues *et al.*, 2013). Given the nature of CFD, variables cannot be explicitly computed at every possible point of the domain, but they are rather approximated. Major aspects of the numerical methods that form the basis of CFD are discussed in section 18.1.2.

19.1.2 How modelling can assist membrane systems

Membrane separation processes (MSP) are operations where a fluid is forced through a thin semipermeable barrier, called a 'membrane'. Transmembrane pressure and electrochemical potential are generally the driving forces used to operate membrane systems (Baker, 2012). One of the key components of MSPs is the membrane itself, as its properties determine the efficiency of separation of the components in the fluid. There are many applications for MSPs such as gas purification, crystallisation and membrane reactors; nonetheless, this chapter focuses on applications in the field of water treatment.

Desalination and tertiary wastewater treatment stand out as the most widely spread applications of membrane systems. These processes are very effective to separate small solutes from water mainly using pressure as the driving force. Nevertheless, they require very high operating pressure (of the order of 10 to 70 bar), which comes with high operation costs. Another issue faced by MSPs is concentration polarisation (CP) which results in a significant decrease in efficiency. CP occurs when the solutes rejected by the membrane accumulate in the vicinity of its surface, forming a region of high concentration, i.e., the concentration boundary layer. Given the nature of MSPs, CP is impossible to prevent, although it can be mitigated so its effect on efficiency is minimised, most commonly via mass transfer enhancement strategies. Other than CP, particulate fouling is also one of the challenging issues that persist in reverse osmosis systems since the technology of RO was first introduced into the desalination process and other pressure-driven operations such as microfiltration, ultrafiltration and nanofiltration.

Over the last decades, CFD has been used to study mass transfer in MSPs and to find innovative approaches to enhance it. Modifying the geometry and location of spacers (Fimbres-Weihs & Wiley, 2008), imposing an unsteady flow at the inlet (Liang *et al.*, 2018b) and vibration-assisted modules (Su *et al.*, 2018), are among the approaches investigated using CFD for mass transfer enhancement in MSPs. Moreover, CFD has also been employed

to study different types of fouling in membrane modules (Fimbres Weihs & Wiley, 2014; Radu *et al.*, 2010). The following sections take a closer look into some specific application cases of CFD analysis of membrane systems.

19.2 METHODS

Using CFD for the analysis of MSPs involves multiple steps that need to be performed to draw valuable conclusions on the model. A comprehensive CFD study comprises three main stages: set-up, solution and conclusion, with an additional stage for experimental validation often performed based on the scope of the study. Figure 1 summarises the typical workflow for CFD modelling. The steps required for setting up the model are in yellow, the ones involved in solving the model are in red and finally, in green, the postprocessing steps. The set-up stage involves the problem definition, generation of the geometry of the fluid domain, definition of the meshing strategy and the establishment of the boundary conditions. Despite seeming trivial, defining the goal and subsequent approach to model a membrane system is crucial, as it sets the foundation of the method.

The solution of the model comes in the next step. CFD uses a numerical approach to solve the Navier-Stokes equations for continuity, momentum and mass transfer. These equations are summarised as follows:

$$\nabla \cdot \vec{v} = 0 \qquad \text{Eq. 1}$$

$$\rho \frac{\partial \vec{v}}{\partial t} + \rho\left(\vec{v} \cdot \nabla\right)\vec{v} = \mu \nabla^2 \vec{v} - \nabla p \qquad \text{Eq. 2}$$

$$\rho \frac{\partial w}{\partial t} + \rho \nabla \cdot (w\vec{v}) = \rho D \nabla^2 w \qquad \text{Eq. 3}$$

where ρ, μ and D are the density (kg m^{-3}), dynamic viscosity (kg m^{-1} s^{-1}) and diffusivity (m^2 s^{-1}), respectively. These physicochemical properties of the fluid are typically considered to remain constant, although, some variations may be caused by temperature and concentration fluctuations. CFD methods solve (numerically) these equations for the velocity vector ($\vec{V}$), the pressure field (p) and the solute mass fraction field (ω).

It is worthy of note that there are currently no generally applicable fully-analytical solutions for the general case of the Navier-Stokes equations, hence the importance of computational methods. Given the numerical nature of CFD methods, they require boundary and initial conditions as inputs to the solution algorithm. Determining a solution to the model is probably the most time-consuming step of modelling, as it involves solving equations - iteratively until the solution error is below a specified tolerance. It is at this point, when the error is sufficiently small and the solution variables are not changing significantly after further iterations, that the solution is said to have converged.

Once the model solution has converged, it should be compared against previous results for the same or a similar model, in a step known as verification. Data processing and assessment come after the results are verified. These two steps are key parts of modelling as they are used to draw conclusion about the model and, ultimately, for decision making. The assessment step is crucial to suggest improvements and correct deficiencies in a real-world system.

Validation is not necessarily part of modelling, although, it is useful to prove that the model is valid for real-world applications. The set-up starts with the problem definition, this is, conceptualising the model that is to be solved. The steps followed for CFD modelling are detailed in the following section.

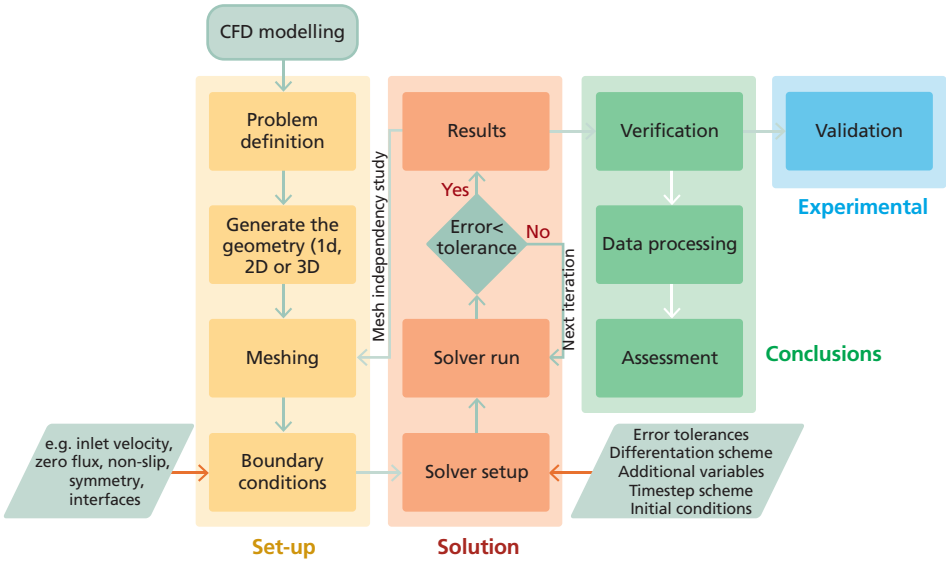

Figure 1 Overall process for CFD modelling of membrane systems.

19.2.1 Geometry

One of the first steps for a CFD simulation of an MSP consists in defining the domain. The geometry of the domain is important as it should represent the system to be modelled. Spirally wound membrane (SWM) modules are the most industrially spread, therefore, many of the CFD models are based in this type of modules. In SWM modules the membrane layers are separated using a spacer mesh with a small width (typically ~1 mm) to create a path for the flow (Scott, 1995). Thus, most CFD analysis of SWM modules consist of domain modelling a spacer-filled narrow channel in order to approximate this geometry. The length of commercial SWM modules is around 1 m which can be difficult to model due to large computational requirements. Nevertheless, the geometry of a SWM module consists of multiple repetitions of small units with the same geometry, called unitary cells. Thus, a common approach in CFD studies is to reduce the length of the channel to be modelled by considering a small number of unitary cells.

Membrane modules can be divided into four categories, namely flat sheet (FS) membrane, spiral-wound membrane (SWM), hollow fibre (HF) and tubular membrane as shown in Figure 2. Among these modules, HF (6000 to 8000 m^2/m^3) is the most compacted (highest surface area per volume), followed by SWM (600 to 800 m^2/m^3), FS (50 to 100 m^2/m^3) and tubular membrane (50 to 70 m^2/m^3) (Martín, 2016). Nevertheless, HF is susceptible to fouling and clogging, thus it can only be used to treat low viscous water (Berk, 2009).

On the other hand, tubular membrane modules have better antifouling properties compared to HF and SWM modules because of their relatively larger diameter (10 to 25 mm), so it can maintain high tangential velocity in the feed stream (Berk, 2009). Thus, it is widely used to treat wastewater with a high content of suspended solids, or viscous oil and water mixtures (Xue *et al.*, 2021). In terms of robustness, the SWM is stronger against the membrane breakage compared to HF (Lu & Chung, 2019). Moreover, FS membranes offer simplicity in design, but they cannot withstand higher pressures, thus they are only suitable for MF and UF (Berk, 2009).

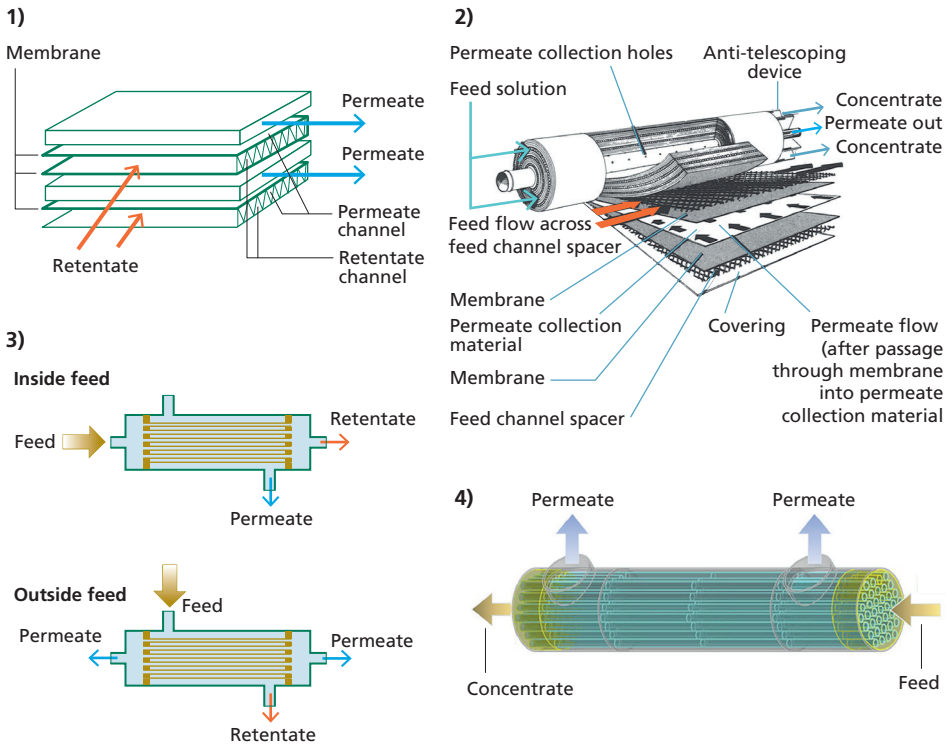

Figure 2 Schematic diagram of (1) flat sheet membrane module (Berk, 2009), (2) spiral-wound membrane module (Sparks & Chase, 2016), (3) hollow fibre module (Balster, 2016) and (4) tubular membrane module (Xue *et al.*, 2021).

19.2.2 Flow types

19.2.2.1 1D, 2D and 3D

As fluid flow is a 3D phenomenon, the most representative way to model it is using a 3D model. However, this may be computationally intensive. In some cases, it is useful to reduce the dimension of the model sacrificing information in order to reduce the computational requirements of a simulation. CFD allows to analyse a system as a 1D, 2D or 3D model and the choice between them depends on the applications intended for a study. For example, a 1D analysis may be useful to analyse a laminar flow between two steady plates, but it overlooks the variations of the flow properties along the other two dimensions. Furthermore, 2D models can be used for flow pattern identification disregarding other phenomena like vortex stretching. In the early stages of CFD, 2D models were the most widely used since the requirements to simulate in 3D were almost inaccessible. Nevertheless, as the capability of computers has improved over the last decades, 3D studies are gaining ground against their 2D analogues (Fimbres-Weihs & Wiley, 2010).

19.2.2.2 Laminar, transient, turbulent

A fluid flow can be classified in different ways according to its characteristics, such as laminar, transient or turbulent. In laminar flow, fluid particles move along a smooth path in parallel trajectories or layers with very low energy losses. On the other hand, turbulent flow is characterised by irregular paths for the flow particles and by large energy losses (Streeter *et al.*, 1985). A fluid flow must have two features in order to be considered turbulent, randomness and auto-similarity (Landahl *et al.*, 1989). Transient flow is an intermediate between laminar and turbulent flow, therefore, it shares some characteristics of these types of flow. Irregular flow trajectory and intermediate energy loss are characteristics of a transient flow.

The hydraulic Reynolds number (Re_h) is almost ubiquitous when characterising a fluid flow. It is the ratio of inertial forces and viscous forces in a fluid flow. The Re_h is described by:

$$Re_h = \frac{u_{eff} d_h \rho}{\mu} \qquad \text{Eq. 4}$$

where u_{eff} is the effective velocity of the flow, d_h is the hydraulic diameter, ρ is the density of the fluid and μ is its dynamic viscosity. A flow with $Re_h > 2100$ is typically considered as turbulent under specific conditions (Rajaratnam, 1976). The hydraulic diameter of the channel is described by:

$$d_h = \frac{4V_{ch}}{a_{ws}} \qquad \text{Eq. 5}$$

The volume of the channel (V_{ch}) and the area of the wetted surface (a_{ws}) depend on the geometry of the channel. Typical values for the d_h are in the order of 1×10^{-3} m.

Operating an MSP under turbulent flow conditions may enhance mass transfer, but implies excessive pressure drop caused by energy dissipation (Burn & Gray, 2015). Conversely, laminar flow may improve mass transfer at relatively low pressure drop. For this reason, most SWM modules operate at a Re_h between 300 and 400 (for reverse osmosis) (Liang *et al.*, 2020b).

19.2.2.3 Single phase

CFD has been used extensively to demonstrate the CP phenomena in a membrane channel for single phase applications. Common membrane applications that involve only liquid phase include desalination and oily-waste water treatment. Since the 2000s, CFD has been used to simulate the hydrodynamic and concentration profiles in the feed channel of SWMs (Fimbres Weihs & Wiley, 2007; Li *et al.,* 2016; Liang *et al.,* 2019) and HFs (Cancilla *et al.,* 2021; Junker *et al.*, 2021; Kaya *et al.,* 2014) for desalination processes. The concentration profile can be visualised in the channel by fixing a solute concentration on an impermeable wall or incorporating Darcy's law on a permeable wall (Pak *et al.*, 2008; Wardeh & Morvan, 2008). As the variations of density and viscosity are insignificant in a horizontal RO membrane system, a Newtonian fluid with constant properties is normally assumed in a SWM feed channel for the purposes of CFD simulation (Foo *et al.*, 2021).

The simulation of oil-in-water MF through CFD approaches has also been presented in the literature (Behroozi *et al.,* 2019; Lotfiyan *et al.*, 2014; Zare *et al.*, 2013). The Eulerian model (described in the following Section) is commonly used to solve the governing equations for the oil and water portions separately. Zare *et al.,* (2013) and Lotfiyan *et al.,* (2014) conducted 2D CFD studies of oil-in-water MF and the simulation could predict the CP profile accurately. However, the permeate flux was underpredicted due to the simplification of the model (e.g., neglecting pore blockage, size distribution of oil droplets, and interaction between oil droplets and the membrane surface). Later, Behroozi *et al.,* (2019) coupled the pore blocking phenomena into a 2D CFD model. The permeate flux predicted by the CFD simulation was comparable to the experiment with 4.62% error. In addition, it was found that the pore-blocking model reduced the relative error by 15% compared to the non-pore blocking model. Thus, considering the pore-blocking phenomena in the simulation of oil-in-water MF can improve the precision of the result.

19.2.2.4 Multiphase

Air sparging in liquid solutions has been extensively used to induce shear stress and mitigate fouling on the membrane surface (Martinelli *et al.*, 2010). This two-phase flow can be modelled using CFD with fluid models such as the Eulerian two-fluid model, or the volume-of-fluid (VOF) model incorporating into the governing equations. In the case of Eulerian two-fluid method, the gas and liquid phases are treated with their respective velocity fields, but both share a common pressure field. Hence, the governing equations are solved separately. VOF model on the other hand, is capable of tracking the gas/liquid interface throughout the computational domain by assuming a no-slip condition between the phases, and that all fluid properties can be calculated as weight-averaged volume fractions (Ndinisa *et al.*, 2005). The governing equations for Eulerian two-fluid (Asefi *et al.*, 2019) and VOF (Javid *et al.*, 2017) methods have been reported elsewhere.

The two-phase flow regime can be either slug or bubbly (Figure 3), which is determined by the superficial velocities of gas phase and liquid phase according to the channel geometry (Golrokh Sani *et al.*, 2021; Gupta *et al.*, 2009). Since the 2000s, modelling two-phase flow in membrane channels through CFD has been extensively studied to understand its impacts on shear stress and flux enhancement (Gupta *et al.*, 2009; Ndinisa *et al.*, 2005; Taha & Cui, 2002, 2006a, 2006b). From the simulation, several approaches were found to be effective for minimizing fouling while enhancing flux such as maintaining high gas flow rate and low liquid rate (Ratkovich *et al.*, 2009), maintaining bigger bubble size (Radaei *et al.*, 2018), and controlled pulse injection (Taha *et al.*, 2006; Taha & Cui, 2002).

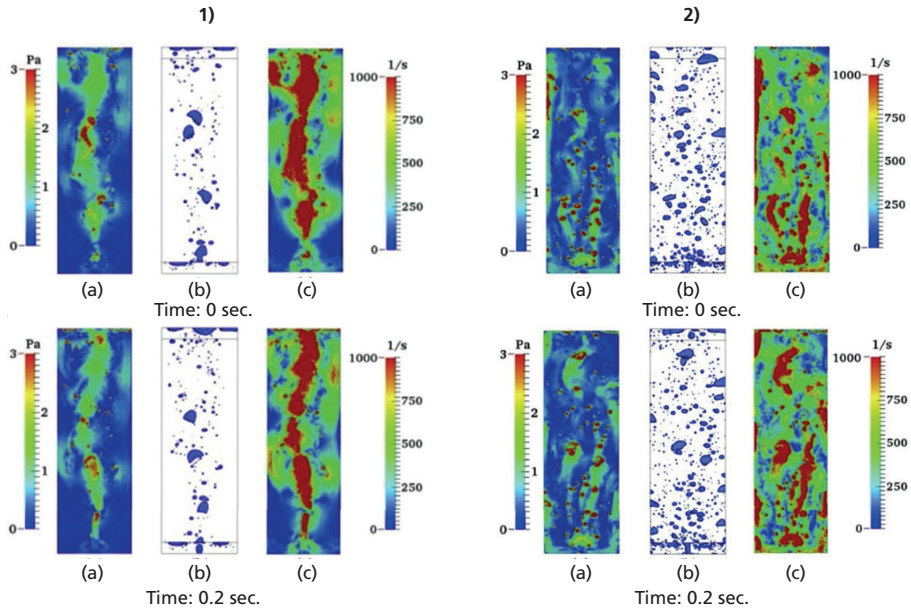

Figure 3 Surface profiles of (a) wall shear, (b) bubbles and (c) vorticity for (1) slug flow and (2) bubbly flow reported by (Javid *et al.*, 2017).

Table 2 Recent 5-years CFD multiphase simulation in membrane process for water treatment

Two phases flow patterns	Software used	Dimension	Modelling approaches	Membrane configuration	Membrane process	Application	Main findings of spacer performances	Ref
Bubbly and slug flows	In-house	2D	Eulerian two fluid	FS	NF	MgSO4 solution	The bubbly flow had marginal impact on the flux enhancement, but a change of the flow regime to slug flow resulted in a flux enhancement.	Asefi *et al.* (2019)
Bubbly and slug flows	OpenFOAM	3D	VOF	FS	UF	whey protein concentrate solution	The velocity gradient of fluid flow near bubbles resulted in the formation of vorticity, which increased shear stress in the membrane system. A significantly larger shear stress was reported in slug flow when compared with the bubbly flow.	Javid *et al.* (2017)
Bubbly and slug flows	ANSYS FLUENT	3D	Eulerian two fluid and VOF	FS	MF	Surface water	Slug flow causes a larger shear stress than the case in bubbly flow. However, the shear induced by bubbly flow was more effective for reducing fouling in pre-treated feed water.	Du *et al.* (2017)
Bubbly flow	ANSYS FLUENT	3D	VOF	HF	MF/MBR	Water and Xanthan gum solution	The fouling rate was found to be inversely proportional to the calculated RMS shear stress. Non-Newtonian fluid showed a reduced tendency in shear fluctuations for membrane cleaning than those observed in water. A larger pulse bubble size yielded more RMS shear stress, which is more effective in fouling control.	Radaei *et al.* (2018)

In recent years, the effects of slug and bubbly flow in a flat sheet channel on shear stress and flux enhancement have been compared through experimental and CFD studies. Air sparging was found to be effectively in reducing the CP by 73% for cross flow NF, leading to flux enhancement (Asefi *et al.*, 2019). However, only slug flow (0.8 min^{-1} to 1 min^{-1}) has significant effects to permeate flux enhancement but not for the bubbly flow (0.2 min^{-1} to 0.6 min^{-1}) (Asefi *et al.*, 2019). Furthermore, an experimental study showed that the slug flow and bubbly flow yield higher flux than single liquid phase flow by 78% and 30% respectively in UF (Javid *et al.*, 2017). This is because the slug flow and bubbly flow result in a higher velocity, which leads to a higher wall shear stress as shown in Figure 3 (Javid *et al.*, 2017). Further, the shear stress caused by the slug flow is higher than those reported in bubbly flow (Javid *et al.*, 2017). In addition, the peak shear stress was found higher for slug flow (15 Pa) than bubbly flow (1.4), although the shear stress is more even distributed for bubbly flow than slug flow (Du *et al.*, 2017). Table 2 summarises recent findings on multiphase for membrane proceses.

19.2.3 Boundary conditions

A set of boundary conditions is required to solve a CFD model due to its numerical nature. Boundary conditions are required at each interface of the model (i.e., inlet, outlet, walls, membrane surface and interfaces). Figure 4 shows a schematic of a membrane channel with the boundary conditions typically used for modelling of MSPs. Other boundary conditions may apply when analysing chemical reaction or heat transfer.

The boundary condition for the incoming flow can be set as inlet or periodic. Setting a flow profile is required for the inlet condition, while a periodic boundary wraps the outcoming flow velocity profile as the inflow. A fully developed profile giving a laminar flow is generally set as the boundary condition at the inlet. The solute concentration profile in the incoming flow can be adjusted according to the application of the model (e.g., constant or periodic). There are three options for boundary conditions at the exit. The outlet condition is the simplest but does not account for backward flow. The opening condition accounts for any recirculation re-entering the channel, but it requires value to be set for any transported variables (e.g., mass fraction and temperature) at the exit. In some cases, the area-averaged concentration at the exit can be calculated and assigned to the backward flow. Setting an opening at the exit usually involves a zero-pressure condition ($p = 0$).

Walls and spacer surfaces are considered impermeable walls with zero-flux, zero-concentration gradient and non-slip velocity conditions. Perhaps the most critical boundary condition is located at the membrane surface, where different approaches may be considered depending on the intended applications.

i. **Impermeable wall with constant concentration**. The concentration at the vicinity of the membrane surface increases due to the CP phenomenon. Under fully developed conditions for the concentration at the membrane surface is roughly twice the concentration at the bulk flow; hence a common assumption includes a constant concentration at the membrane surface. Other assumptions made include a zero flux throughout the membrane (impermeable wall). This assumption is not realistic for MSPs, but it has been shown that the flux across the membrane has very low impact on the

characteristics of the boundary layer (Schwinge *et al.*, 2002b). In addition, the flux across the membrane may be estimated using a correlation developed by Geraldes and Alfonso (2006). These considerations are useful to analyse the mass transfer and hydrodynamics inside the channel while reducing computational time.

ii. **Semi-permeable wall**. This is a more realistic approach to membrane systems modelling as it accounts for the separation capacity of the membrane (Ahmad *et al.*, 2005). In this case, the flux throughout the membrane is computed using the physicochemical parameters of the membrane such as permeance and intrinsic solute rejection. This model is suitable for cases where the ratio between permeate flux and bulk flow velocity is higher. Calculating the flux is especially important for techno-economic assessment since it is used to determine the productivity of the system.

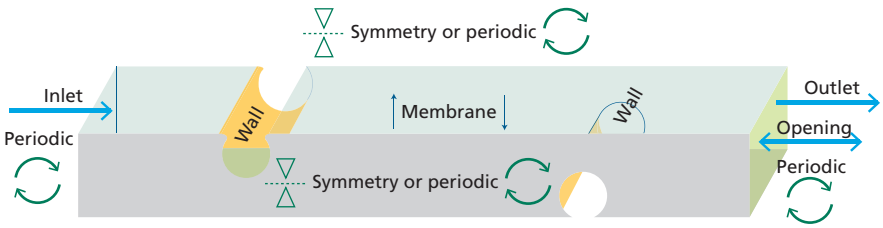

Figure 4 Schematic of a narrow spacer-filled membrane channel and possible boundary conditions for CFD analysis.

19.2.3.1 Steady-state and transient-state

There are two types of CFD simulations that can be used to model membrane systems, steady- and transient-state. The solution obtained in a steady-state simulation describes the behaviour of the system in the long term, when there is no variation over time ($dw/dt = 0$). In general, the variables of the system are recalculated over the domain until some convergence criterion is reached. Steady-state simulations require relatively low computational time; therefore, they are suitable for most of the engineering problems where the goal is to determine the final state of the system.

Transient-state simulations are used to determine the evolution of a system over time. These provide more information on the phenomena taking place in a membrane system and can be used for fundamental analysis (e.g., flow pattern analysis). In transient-state simulations a steady solution is computed at each timestep which involves large computational time.

19.2.4 Initial conditions

The finite volume method requires an initial condition for each element as any numerical method. The selection of the initial condition is normally based upon previous information on the model and using an arbitrary set of initial conditions may lead to excessive computational time. Using a good approximation of the transient-state as an initial condition can significantly speed up the simulations. This can be achieved by setting a previous steady-state solution as the initial condition for the transient case.

19.2.5 Meshing and algorithms

CFD is essentially a numerical technique that commonly uses a finite volume scheme to calculate the properties of the flow within the domain. The finite volume method is based on discretising the fluid domain in a finite number of smaller volumes, which collectively form the mesh. All assigned variables are calculated for these elements and some interpolation scheme is used to estimate their values at mid-points. The mesh can be structured or unstructured depending on requirements of the application. In a structure mesh the elements share the same pattern of construction, whereas in an unstructured mesh has multiple patterns. Unstructured meshes are typically suitable to model MSPs since mass transfer occurs differently at different locations of the domain. For MSPs, more elements are required at regions where the concentration gradient is higher, such as close to the membrane surface. The structured mesh is useful for regions where the flow is tangential to the boundary. Most CFD models combine both types of meshing to increase the resolution of the method at a low computational time. Figure 5 shows an example of the mesh used for CFD modelling including an unstructured pattern for the bulk flow region and a structured pattern for the region corresponding to the boundary layer (zoomed-in). A coarse mesh is shown as an example for better visualisation; however, it is recommended that meshes where the largest elements are about 5% of the channel height are used for CFD studies of membrane channels under typical operation conditions.

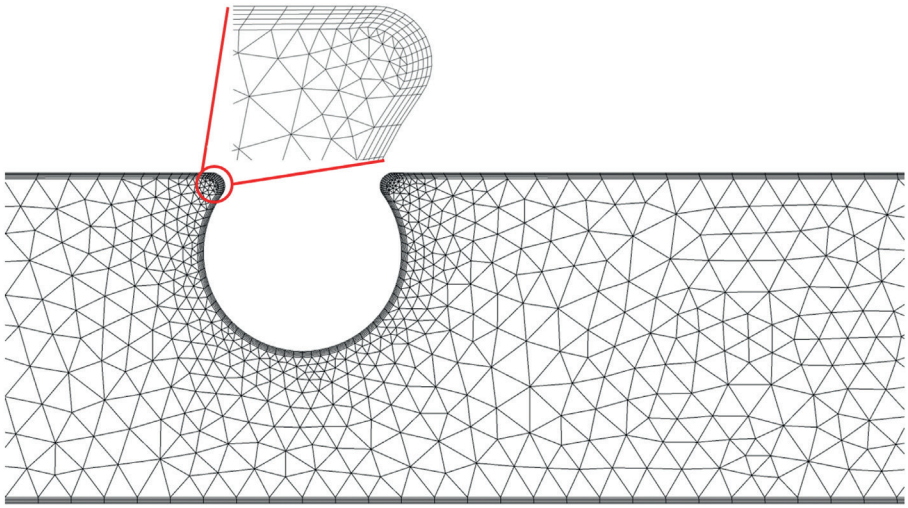

Figure 5 Typical meshing approach for mass transfer analysis on a narrow membrane channel using CFD.

Another meshing approach is using an adaptive mesh, which changes with every iteration on an established criterion. The solute concentration gradient may be used as a refinement criterion as it is advisable to have more elements in the regions with higher mass transfer. When using adaptive meshing the software will automatically refine those regions where the criterion is met at a certain number of iterations. Using adaptive refinement increases the

computational time required to solve each iteration, however, it can reduce significantly the number of iterations required by the model. Both steady-state and transient-state cases can be solved using adaptive meshing on ANSYS FLUENT and ANSYS CFX.

19.2.6 Convergence

The results obtained via CFD simulation change with every iteration or timestep and a criterion is required to determine when to stop the simulation. The convergence criterion for steady-state simulations is the residual which measures the imbalance of a conserved variable for each control volume (ANSYS Inc., 2021). Given the numerical nature of the method, the residuals cannot be zero, but an acceptable tolerance is set arbitrarily depending on the precision required for the analysis. The residual tolerance can be set as maximum or root mean square (RMS) with the former being stricter. A solution is considered converged when the residual is equal or less than the tolerance setpoint. The residuals of the velocity and pressure fields are computed by default in most of the commercial software, however, the user can add additional criteria for other variables. It is important to note that using stringent criteria for the residual, can significantly increase the required computational time.

The velocity and pressure fields are typically sufficient to determine convergence in terms of hydrodynamics, but not for mass transfer. Additional variables such as solute concentration or mass transfer coefficient are suitable as a convergence criterion when analysing mass transfer phenomena.

Transient-state simulations require the solution to be converged in time, therefore, the relative error is computed between two different time-dependant states of the system, often referred as 'snapshots'. The error between two snapshots depends on the timestep size; for example, using a very small timesteps will misleadingly reduce the relative error significantly. The ratio between the relative error and the timestep size, which is analogous to the time derivative, may be used to account for the effect of the timestep size. Another approach is to compute a time-averaged variable within a time window and use it as convergence criterion. The later approach is useful for oscillatory states where the variables are not converging to a single value over time, but rather they oscillate within a limit cycle.

19.3 DATA ANALYSIS

19.3.1 Verification

Another essential step of CFD modelling is the verification of the results. At this stage we already have precise results and now the main goal is to determine whether they are accurate or not. Verification is done by comparing the results obtained against some previously reported for a same (or similar) model or method. In most of the cases there is no true value to aim for, unless there are explicit analytical solutions available for the variables to be compared. Instead, there is a range within the results are considered acceptable. The results used for verification are commonly the area-averaged Sherwood number ($\overline{\mathrm{Sh}}$) and the global friction factor (f_{glob}), which are indicators of mass transfer and energy loss, respectively. The $\overline{\mathrm{Sh}}$ and the f_{glob} are described by the following equations:

$$\overline{Sh} = \frac{d_h}{w_w - \frac{1}{2}\left(w_{b,out} - w_{b,in}\right)} \left(\frac{\partial w}{\partial y}\right)_{w,AA} \quad \text{Eq. 6}$$

$$f_{glob} = \frac{d_h}{2\rho u_{ave}^2} \frac{\Delta P}{L} \quad \text{Eq. 7}$$

In Equation 6, w_w is the solute concentration at the membrane surface and, $w_{b,out}$ and $w_{b,in}$ are the solute concentration at the bulk at the outlet and the inlet, respectively. The partial derivative term is the area-average of the y-component of the solute concentration gradient vector at the membrane surface (m^{-1}). Moreover, in Equation 7, ρ is the density of the fluid (kg m^{-3}), u_{ave} is the average velocity of the bulk flow (m s^{-1}), ΔP is the pressure drop across the channel (kg m^{-1} s^{-2}) and L is the channel length (m). Despite being good indicators of the channel performance, using $\overline{Sh}$ and f_{glob} for verification, overlooks the local aspects of the flow.

Another type of verification that is typically carried out in CFD modelling is mesh independency analysis. Mesh independency studies are used to quantify the error introduced by the meshing strategy by computing the flow variables using different meshes. The error for a variable is computed for meshes with different number of elements until certain tolerance is reached. The variables selected should be representative for the whole domain and for the phenomena that is being studied (e.g., hydrodynamics, mass transfer or heat transfer). In addition, the effect of the number of elements should be taken into account as, for example, the error between two meshes may be small because they have relatively the same number of elements. First developed by Roache (1997), the grid convergence index (GCI) is one of the first introduced criterion for mesh independency studies as it accounts for the entire domain and for the number of elements of the mesh. The GCI for a fine mesh (GCI_{fine}) is described by:

$$GCI_{fine} = \frac{3|e|R^{\eta}}{R^{\eta} - 1} \quad \text{Eq. 8}$$

where η is the order of accuracy (or the dimension number), e is the relative error for an integral function between two meshes and R is the growth factor for the number of elements. Values for the GCI_{fine} less than 5% are typically considered acceptable but, of course, this depends on the application of the model. Although this criterion is very suitable for structured meshes, it presents some issues when used for unstructured meshes, as increasing the number of elements does not necessarily decrease the error. Refining in regions where the gradients (either velocity or concentration) are very small may cause an 'artificial' decrease in the GCI, while increasing the number of elements in a relatively small amount can lead to a higher GCI.

The GCI as a verification metric has more recently been replaced by alternative criteria for mesh independency analysis, as it has been shown that unstructured meshes are more suitable for modelling membrane systems. Recent CFD studies focus on the behaviour of

integral functions (e.g., $\overline{Sh}$ and f_{glob}) in an effort to circumvent the effect of the number of elements of the mesh on the GCI. A typical approach consists in computing these integral functions for multiple discretisation meshes with an increasing number of elements, while also computing the relative error between each other until an asymptotical behaviour of the integral function is observed. An arbitrary threshold for the relative error is set depending on the level of accuracy required for the study, with 5% being acceptable for most applications. It is important to highlight that this verification approach requires using the same meshing strategy for all the meshes compared.

19.3.2 Validation

Validation assessment determines if the computational results agree with physical reality (NASA, 2022). The results obtained throughout a CFD simulation are compared against experimental data in order to validate them. In another words, validation is used to determine if the computational model is actually representative of the physical system that was intended to analyse. Some physical systems may be very difficult to setup or to monitor, this is why in some cases CFD analysis comes before and its validation can become an issue. In these cases, the validation may be performed by comparing against experimental results from a different model with similar characteristics.

Existing techniques for experimental analysis of flows include particle image velocimetry (PIV), micro-particle image velocimetry (μPIV) and holographic particle image velocimetry (HPIV). These techniques use optical devices such as lasers, cameras and lenses to capture the flow pattern structures in the fluid. PIV is based on the light scattering capacity of small particles that often need to be added to the fluid. A high-speed camera captures snapshots of the tracer particles distribution to visualise the flow pattern (Lindken & Burgmann, 2012). μPIV refers to the PIV variation where the fluid motion can be determined by the resolved length scales, ranging from 10^{-4} m to 10^{-7} m. A specialised high-resolution camera is required to achieve microscopic length scales for μPIV. The application of μPIV include visualisation of fluid patterns in microchannels, which makes this technique suitable for flow analysis in membrane narrow channels. Figure 6a shows the typical components of the experimental set-up for PIV and μPIV. A flow field captured using PIV is shown in Figure 6b.

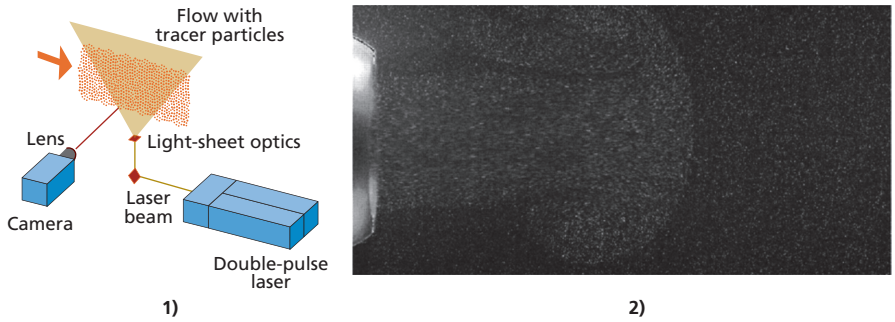

Figure 6 (1) Experimental set-up for PIV/μPIV (Lindken & Burgmann, 2012) and (2) jet flow image captured using PIV (Yu *et al.*, 2021).

HPIV stores the amplitude and phase of a light wave in a two-dimensional film, the hologram. Based on the wave interference phenomenon, the interference pattern of this scattered wave is compared against a second wave refer to as the reference wave (Hinsch, 2002). The interference pattern is then used to reconstruct the flow field by illuminating the hologram with a replica of the reference wave. Figure 7a depicts a basic set-up for HPIV with its components. In general, the laser beam is split into an object wave and a reference wave using an arrange of optical devices. The object wave is directed towards the flow and the reference wave to the holographic film (or device, for digital HPIV). Figure 7b shows an example of a HPIV hologram, whereas the corresponding particle distribution is shown in Figure 7c (Sun *et al.*, 2020).

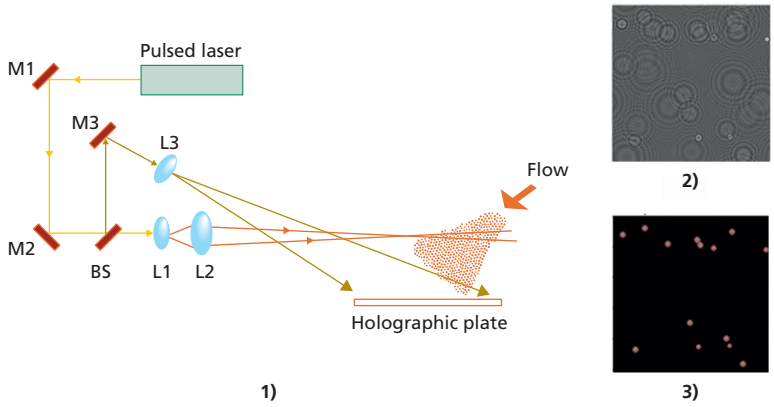

Figure 7 (1) Schematic of a HPIV set-up (Bryanston-Cross *et al.*, 1992), (2) hologram of an interference pattern and (3) corresponding particle distribution (Sun *et al.*, 2020).

Despite the excellent performance of the aforementioned experimental methods for flow characterisation, the applications for membrane systems are limited. For example, the small solutes (salts or organic molecules) common in membrane systems are difficult to emulate for PIV since, the latter requires particles to have certain characteristics to be able to scatter light.

19.4 DATA DISCUSSION AND INTERPRETATION

19.4.1.1 Data processing and assessment

Simulations may yield large amounts of data and their interpretation is often the cornerstone of CFD analysis. Numerical data has very little to no value if it is not processed and interpreted correctly to draw information about a physical system, as that is the purpose of CFD modelling. When presenting results, data is most often used to verify or validate the model, to explain physical phenomena taking place in the system or to propose improvements. CFD may also be coupled with different mathematic tools such as, calculus, Fourier analysis, statistics and linear algebra to produce valuable data for membrane system modelling. In addition, data science (Holemans *et al.*, 2022) and machine learning (Vinuesa & Brunton, 2022) are increasingly used to make CFD a more powerful tool for modelling.

19.5 APPLICATIONS, EXAMPLES

19.5.1 Flow stability

19.5.1.1 Laminar steady

The first uses of CFD for membrane modelling where focused on optimising the design of mesh spacers (Da Costa *et al.*, 1994). These studies used laminar flow in spacer-filled membrane channels to gather information about the CP phenomena. Cao *et al.* (2001) found that recirculation zones are formed before and after the spacers in a narrow membrane for laminar flow. The presence of recirculation zones significantly increases the mass transfer enhancement as they introduce low concentration flow to the boundary layer. Nevertheless, the effect of recirculation zones on mass transfer is limited as they remain attached to the boundary and eventually stabilise. Ahmad *et al.* (2005) went a step further by studying the mechanism by which the recirculation zones increase mass transfer, finding that increasing the shear rate at the membrane surface is critical to mitigate CP. As the role of shear rate (velocity in the normal direction) on the boundary layer development became more evident, the efforts were diverted towards finding ways to destabilise the boundary layer by increasing shear rate.

19.5.1.2 Laminar unsteady – oscillating vs vortex shedding

The fluid flow pattern may change over time under specific conditions without being considered turbulent. This flow regime is called laminar unsteady and it is characterised by unsteady recirculation zones. Recirculation zones may contract and expand or move while remaining attached to the wall affecting the boundary layer. Figure 8a shows a flow pattern for a recirculation zone. Destabilising recirculation zones may cause them to detach and get convected by the bulk flow in a phenomenon called vortex shedding. The efficiency of vortex shedding to mitigate CP is higher than that of recirculation zones as these only affect a small portion of the channel. Vortex shedding is characterised by two separate regions with swirl motion with one of them detaching from the boundary and moving downstream. The double swirl pattern for vortex shedding is shown in Figure 8b.

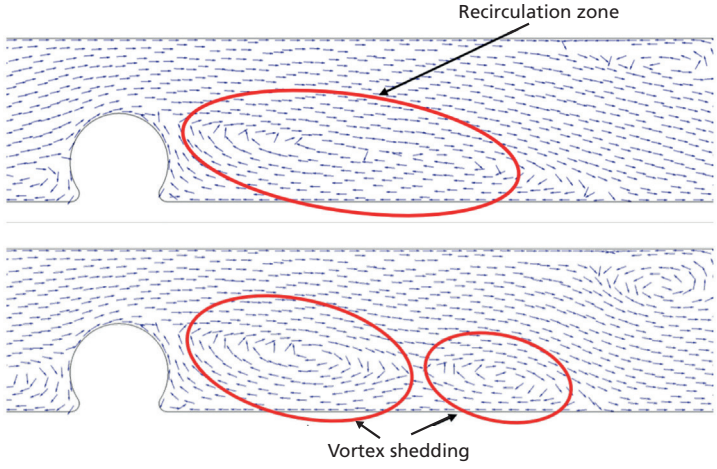

Figure 8 Fluid flow patterns for (top) recirculation zones and (bottom) vortex shedding in a spacer-filled membrane channel (Fimbres-Weihs *et al.*, 2006).

Vortex shedding occurs in flows at higher Reynolds number translating into more energy requirements. Because of this, some researchers have focused on finding the optimal Reynolds number that can cause vortex shedding, but at a lower energy requirement. Alexiadis *et al.* (2007) found that the critical Reynolds number (Re_{cr}) for the transition from recirculation zones to vortex shedding in spacer-filled membrane channels is within the range of 526-841.

Fimbres-Weihs *et al.* (2006) studied mass transfer under unsteady-flow conditions at hydraulic Reynolds numbers up to 1683, paying special attention to the causes of mass transfer enhancement. Wall shear was identified as having a significant impact on mass transfer enhancement; however, the inflow of lower concentration towards the membrane surface was found to dominate mass transfer phenomena. Thus, recent CFD studies on mass transfer enhancement are focused on maximising the inflow towards the membrane surface (i.e., normal velocity).

19.5.1.3 Quasiperiodic flow

The study of fluid flow instabilities is crucial as the effect of disturbance on the hydrodynamic stability and how the flow system responds to it remain unclear. Fluid periodicity is one of the indicators to measure the flow stability. Fluid periodicity in flow refers to a flow system that displays a recurring behaviour given at regular intervals. Quasiperiodic flow, on the other hand, refers to a recurrence behaviour with a component of uncertainty, such that it could be periodic on a small scale but unpredictable on a large scale, which would eventually result in imprecise measurements.

From fluid mechanic point of view, the flow can be classified into three states namely the laminar, transition and turbulent flow. The fluid flow states are usually determined by a dimensionless number known as Reynolds number. Reynolds number (*Re*) is defined as the ratio of inertial forces to viscous forces in a fluid flow. As *Re* increases, the inertial forces become larger, leading to flow instability (Masuda & Tagawa, 2019). Transition flow is a mixture of laminar and turbulent flow occurring simultaneously in a fluid channel with a range of *Re* between 2,000–4,000. During the transition state, aperiodic oscillatory flow or quasiperiodic flow usually occurs due to the unstable flow condition with mixed characteristics of laminar and turbulent flow characteristics. Nowadays, Computational Fluid Dynamics (CFD) has been widely used to study the hydrodynamics behaviour of quasiperiodic flow. One of the advantages of flow simulation by CFD is that it can help to generate different physical data such as vorticity or energy dissipation rate which cannot be measured easily in practical experiments.

Schwinge *et al.*, (2002a) investigated the effect of unsteady 2D flow in narrow spacer-filled channels for spiral wound membrane modules. Their simulation results show that when the membrane channel is filled with obstacles (spacer), an unsteady flow pattern is observed at *Re* as low as 200, depending on the geometry of the obstacles. Figure 9 shows the transition of flow from stable to unsteady conditions occurring at *Re* above 300 for a single filament located at the centre of a narrow channel. At this Reynolds number, the recirculation begins to form behind the filament and as *Re* increases, the extent of flow unsteadiness increases until it reaches a turbulent condition. For a single filament located close to the bottom wall, the flow is found to be stable for *Re* below 600 and it becomes unstable when Re increases

above 600 as the flow disturbance induced by the recirculation behind the filament spreads the unsteadiness downstream the membrane channel (as shown in Figure 10). Nevertheless, their transient results also found that the channel walls close to the cylindrical filament tend to stabilise the fluid flow and slow down the transition of flow to the unsteady state.

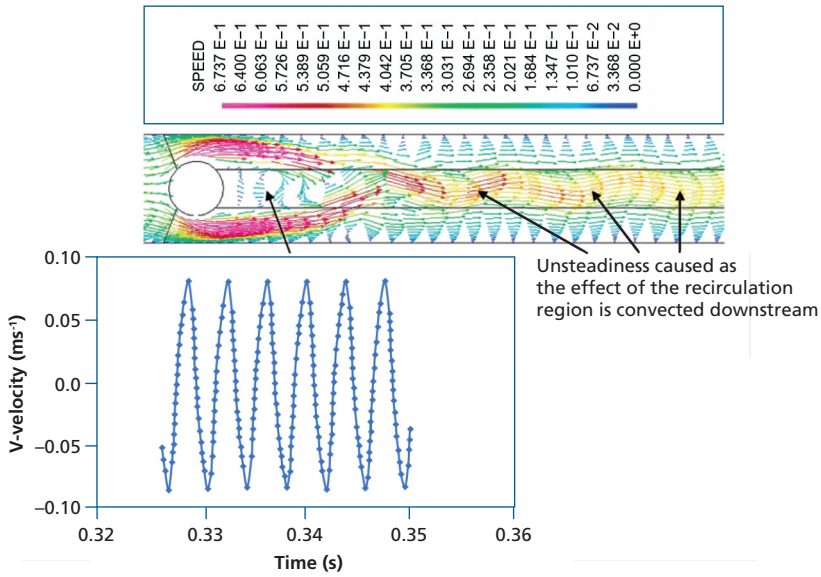

Figure 9 Unsteady flow caused by a cylinder located in the centre of the narrow channel for Re = 500 (Schwinge *et al.*, 2002a)

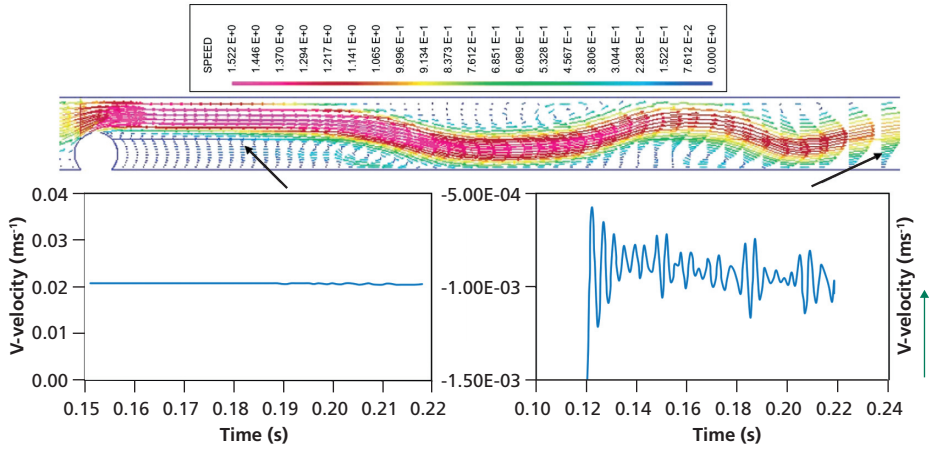

Figure 10 Unsteady flow caused by the cylinder close to the bottom wall for Re = 1,000 and small flow disturbances are convected downstream (Schwinge *et al.*, 2002a)

19.5.1.4 Turbulent flow

Turbulent flow generally occurs at a Reynolds number greater than 2,000. As Reynolds number increases, the fluid flow undergoes irregular fluctuations or mixing that eventually leads to an aperiodic oscillation. Not only that, the direction and magnitude of fluid flow are constantly changing at a turbulent condition. The characteristics of a turbulent flow include higher velocities, low viscosity and higher characteristic linear dimension compared to a laminar flow. Due to the random nature and irregularity of turbulent flow, the flow pattern is extremely difficult to understand. Hence, the governing equations for turbulent flow condition are not easy to develop due to the unsteady flow continuously changing with time, which increases the difficulty level for studying flow turbulence. Although the analysis of turbulent flow is very challenging, analysis of flow turbulence is important for industries as currently there are more membrane filtration processes are using turbulent flow to enhance mixing and reduce the extent of concentration polarisation in the membrane module.

In general, there are three main ways to simulate turbulent flow using CFD technique, including the Direct Numerical Simulation (DNS), Large Eddy Simulation (LES), and Reynolds-Averaged Navier-Stokes (RANS) equations. The computational cost associated with solving the flow simulation increases ascendingly with the order of RANS, LES, followed by the DNS technique in CFD modelling. For DNS and LES methods, CFD will take into account the majority of fluid scales in simulation and provide a comprehensive flow data. In contrast to DNS and LES, RANS do not require fine details of all the turbulent eddies, hence lower computational cost. However, the accuracy of flow simulation can be impacted for RANS method because the flow is only simply modelled and not fully (DNS) or partially (LES) resolved.

Jafarkhani *et al.* (2012) developed a 3D model with semi-circular baffles incorporated into the membrane tube to study the hydrodynamic behaviour of turbulent flow. Their results found that the intense fluctuations induced by the baffles increase the local wall shear stress and velocity in the membrane channel. The induced turbulence to the bulk flow at *Re* up to 7,500 results in a rapid change in the flow directions, which enhances the flow fluctuations and reduces the formation of concentration boundary layer on the membrane surface, consequently leading to a potential fouling reduction while improving the filtration flux performance.

19.5.2 Mass transfer and vortex shedding

Vortex shedding occurs as an oscillating flow at specific velocities when a fluid flow passed a bluff body depending on the size and shape of the body. The alternate formation and shedding of vortices produce alternating forces, which happen more frequently as flow velocity increases. This phenomenon plays a vital role in membrane technology due to the significant impact of vortex shedding on membrane efficiency, as well as the mass and heat transfer of a fluid flow passed a bluff body (Korinek *et al.*, 2017). Research has shown that vortex shedding is capable of enhancing membrane separation efficiency by increasing the transmembrane flow, while disrupting the formation of thermal and solute boundary layer on the membrane surfaces.

Su *et al.*, (2018) investigated the performance of a vibration-enhanced reverse osmosis membrane module on the membrane separation efficiency. Their CFD results showed that the vibration force results in more vortices along time at the downstream and upstream faces of the membrane, compared to that of non-vibration case (Figure 11). The vortex generation induced by the vibration increases the boundary shear rate in the membrane channel, which significantly reduces CP.

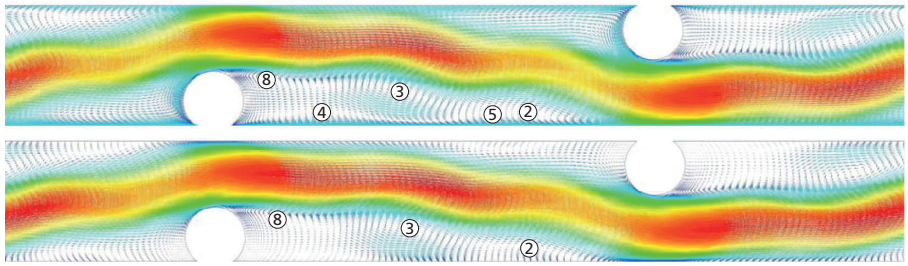

(c) t = 5 ms

Figure 11 Velocity vector profile of vibration case (top) and non-vibration case (bottom) (Su *et al.*, 2018).

19.5.3 Spacer design

19.5.3.1 Two-Dimensional Feed spacer

The accumulation of solute due to membrane rejection leads to concentration polarisation (CP), which later causes the deterioration of membrane flux. Thus, intensive studies such as optimisation of feed spacer geometry in the membrane channel have been performed to mitigate CP by enhancing the mixing of fluid. The first two-dimensional (2D) models of spacer-filled membrane channels appeared in the early 2000s, aiming to understand its hydrodynamic (Chong *et al.*, 2022a) and concentration profiles. Later, the configurations of the spacer (e.g., cavity, submerged and zigzag) and other parameters (filament diameter, mesh length, etc.) have been studied thoroughly to understand their impacts to the flux enhancement and pressure loss.

Early 2D feed spacer study found that zig-zag spacer was the most efficient spacer for SWM module (Schwinge *et al.*, 2002b). Subsequent findings include 1) dependence of formation of recirculation region on spacer geometry and flow condition (Schwinge *et al.*, 2002a); 2) significance of vortex shedding for mass transfer enhancement. It was also concluded that the mass transfer enhancement depends on two important mechanism: 1) flow of low solute concentration to the membrane boundary layer and 2) increase of wall shear (Fimbres-Weihs *et al.*, 2006).

19.5.3.2 Three-Dimensional Feed Spacer

3D modelling of spacer-filled channel emerged rapidly around 2010 due to improvement of computer processing and storage of capacity. During the first decade of 21st century, the research direction regarding CFD analysis in spacer studies mainly focused on the hydrodynamic performance caused by the spacer. Later, the effect of various geometries such

as the filament size, mesh length and flow attack angle on the mass transfer performance and pressure loss reduction were studied and investigated (Gu *et al.*, 2017). In the past decade, the research direction concerning CFD analysis of spacer-filled channels has shifted and focused more on the novel spacer geometries for further improvement on the mass transfer performance and reduction in the pressure loss (Park *et al.*, 2021).

Chong *et al.* (2022) studied the effects of submerged spacers with variations in the node geometries and sizes (as shown in Figure 12a) on the hydrodynamics and mass transfer performance through CFD. It is found that conventional spacers have similar or higher Sh than the submerged type spacers at lower Re_h (<100) because of the sideway flow. However, due to a greater vortex mixing effect, submerged type spacers performed better than the conventional spacers at higher Re_h (>200). In addition, the mass transfer performance of the spherical node spacer is inferior to the column node spacer as the flow can pass through the gap between the spherical nodes and membrane, thereby resulting in a lower local velocity at filament and mass transfer. In fact, as node size increases, pressure loss increases as well because of the larger nodes significantly impeding the flow, creating more form drag and skin friction in the membrane channel, thus increasing the pressure loss.

Recently, a honeycomb shape spacer (Figure 12b) was proposed in which it has the ability to generate high-magnitude turbulent kinetic energy in the area of spacer filaments, resulting in a smaller fouling deposit (Park *et al.*, 2021). Furthermore, optical coherence tomography (OCT) scans showed the fouling layer thickness could be decreased by 33% using the honeycomb spacer.

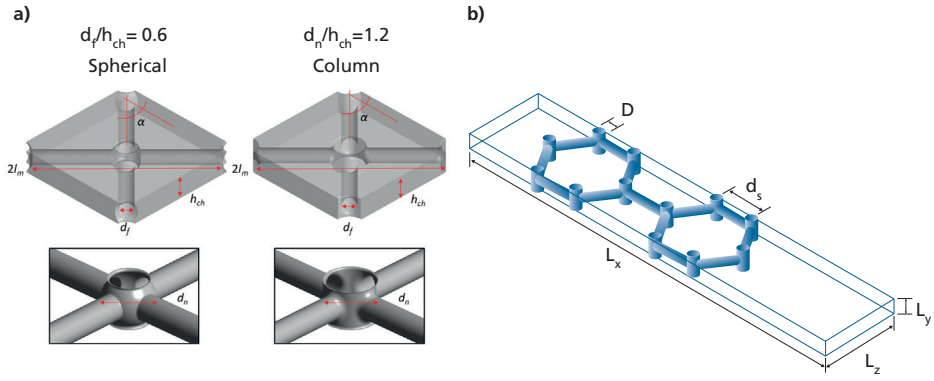

Figure 12 Schematic diagram of (a) spherical nodes submerged and column nodes submerged spacers and (b) honeycomb spacer (Park *et al.*, 2021)

19.5.4 Flow perturbation

One of the efforts to minimise concentration polarisation (and eventually fouling) in a membrane system is by introducing a disturbance into the fluid flow through an external flow perturbation technique. With the help of CFD, the technique is performed in an attempt to induce flow unsteadiness for promoting fluid mixing and therefore, reducing the fouling tendency in membrane modules (Fimbres-Weihs *et al.*, 2006; Schwinge *et al.*,

2002a). The flow perturbation technique generally involves creating unsteadiness to the bulk flow, which can be done by introducing an oscillating flow to the system; or causing a disturbance to the boundary layer adjacent to the membrane surface by using vibration or electro-osmosis approach. Further descriptions regarding the flow perturbation techniques as well as their effectiveness in enhancing membrane performance are elaborated in the following sections.

19.5.4.1 Electro-osmosis

Electro-osmosis is an electrokinetic phenomenon involving the movement of a thin fluid layer adjacent to a charged surface in response to an external electric field (Asadi *et al.*, 2013; Hu & Li, 2007; Jagannadh & Muralidhara, 1996; Ouyang *et al.*, 2013). The electrokinetic phenomenon occurs due to the electrostatic interaction between the similarly charged and oppositely charged ions in the vicinity of a solid/liquid surface, which then results in the motion of a thin fluid layer near the surface, as illustrated in Figure 13. Electro-osmosis has great potential to enhance mass transfer while minimising fouling tendency, particularly for membrane separation processes, such as reverse osmosis and nanofiltration because a disruption to the flow near the membrane surface tends to promote back-transport of solute and reduce polarisation effect (Liang *et al.*, 2014a). Further, the approach is suitable for water treatment and desalination processes as there are salts and charged species involved in the system that can respond to the applied electric field (Jagannadh & Muralidhara, 1996).

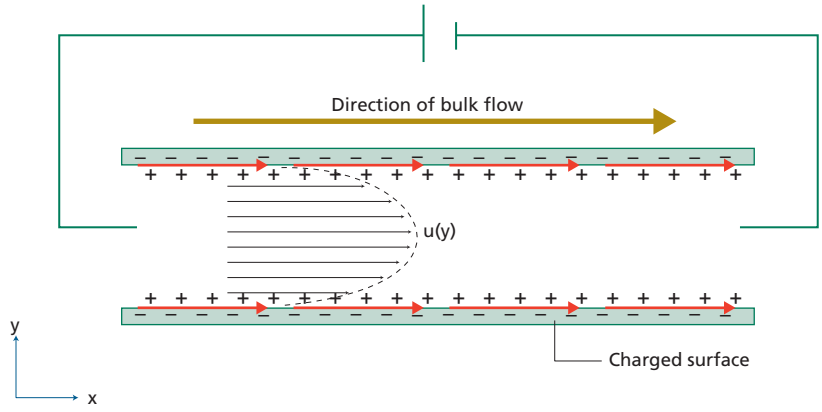

Figure 13 Schematic of electro-osmosis technique with red arrows representing the electro-osmotic flow (EOF) adjacent to a charged surface in an empty flow channel.

Several theories have been developed to describe electro-osmosis, including the Helmholtz-Smoluchowski (HS) theory, the Spiegler friction model, the Schmid theory, and ion hydration theory. Among those early theoretical approaches, an early study of Spiegler and Macleish (1981) investigated the electro-osmosis technique on a reverse osmosis desalination process by filling the feed stream with ferric hydroxide. Their results showed that the electro-osmotic backwashing of the membrane managed to recover a range of 30–100% of flux loss in the system. Despite the great potential of electro-osmosis, the technique is difficult to analyse experimentally in a membrane system due to various technical

constraints. Hence, there is significant value in utilising CFD as a tool for understanding the mechanisms of electro-osmotic flow (EOF) in enhancing mass transfer and fluid flow in a membrane process. The following sections further discuss the modelling of electro-osmosis in membrane system studies and the many learnings obtained using CFD.

19.5.4.2 Modelling electro-osmosis in CFD

Electro-osmotic flow refers to the motion of a thin fluid layer that carries a net electric charge acting upon a fluid/solid interface (i.e., membrane surface) in response to an electric field. This layer of net charge is known as the electric double layer (EDL) and is often characterised by the Debye length (λ_D) (Cummings *et al.*, 2000), which is formed due to the charge separation occurred near the fluid/solid interface. The movement of fluid layer (EOF) is then driven by the excess charged ions in the double layer field via viscous effect under the influence of external electric field (Hu & Li, 2007; Probstein, 1989; Russel *et al.*, 1991). For an incompressible fluid flow in a membrane system, the electro-osmotic effects can be introduced into the Navier-Stokes momentum equation by means of an external force given as follows (Hu & Li, 2007):

$$\rho\frac{\partial\vec{v}}{\partial t}+\rho\left(\vec{v}\cdot\nabla\right)\vec{v}=\mu\nabla^2\vec{v}-\nabla p+\rho_e\vec{E}+\rho g \qquad \text{Eq. 9}$$

where ρ, $\vec{v}$, p, μ, ρ_e, $\vec{E}$, and g are the density, velocity vector, pressure, fluid viscosity, electric charge density, electric field, and gravitational acceleration, respectively. The electric field ($\vec{E}$) can be calculated as follows:

$$\vec{E}=-\nabla\left(\phi+\psi\right) \qquad \text{Eq. 10}$$

where ϕ and ψ are the potentials due to the double layer and external electric field, respectively (Patankar & Hu, 1998; Rawool & Mitra, 2006). The charge density (ρ_e) can be related to the electric potential by the Poisson equation (Hunter, 2013):

$$\nabla^2\phi=\frac{-\rho_e}{\varepsilon} \qquad \text{Eq. 11}$$

where ε is the fluid permittivity. Excluding any disturbance to the double layer, the charge density can be solved by the Boltzmann distribution or other similar correlations (Hunter, 2013; Probstein, 1989).

Nevertheless, the high computational requirement and cost is one of the challenges for solving the Poisson and Navier-Stokes equations at the scale of Debye length ranging up to several hundred nanometres in numerical simulation of electro-osmosis considering a typical membrane channel height of ~10^{-3} m. For the sake of simplicity, the thickness of double layer is generally assumed to be neglected in most EOF studies (Hu & Li, 2007). In fact, the coupled relations between the Poisson and Navier-Stokes equations can be simplified by dropping the EOF term $\rho_e\vec{E}$ from equation 9 and instead, replace the no-slip boundary condition at channel surfaces by using the Helmholtz-Smoluchowski (HS) slip boundary (Anderson, 1989; Hu & Li, 2007; Ren *et al.*, 2003; Santiago, 2001; Zhang *et al.*, 2006).

Using the simplified HS approximation, the electro-osmotic flow can be incorporated as an artificial forced slip velocity applied along the surface of the membrane channel in a separation module. The HS slip velocity is applied outside the edge of the double layer assuming the thickness of EDL much smaller compared to the channel height (Probstein, 1989). In addition, the slip velocity equation assumes a 1D charge distribution when the fluid velocity is small and/or the inertial terms in the momentum equation do not dominate (Patankar & Hu, 1998). Assuming time constant with negligible pressure gradient and gravitational acceleration, the coupled system of Poisson and Navier-Stokes equation from equation 9 can be simplified to the following HS equation, which corresponds linearly with the magnitude of electric field, expressed as follows (Probstein, 1989):

$$u_s = -\frac{\varepsilon \zeta E_x}{\mu} \qquad \text{Eq. 12}$$

where u_s is the forced slip velocity, ζ is the zeta potential, and E_x is the magnitude of electric field in the x-direction. The permittivity (ε) is assumed to be uniform for the case of an RO system, such that the permittivity value of the membrane can be regarded as similar to that of water (Liang *et al.*, 2014a). This is because of the structure of RO membrane which is mostly comprised of the high porosity support layers (Antony *et al.*, 2013), along with an extremely fine selective membrane layer of 1×10^{-7} m or less (Baker, 2004), in order to assume a uniform permittivity value and to safely neglect any effect related with the nonuniformity in this case.

The HS approximation was compared against a more rigorous charge density distribution (CD) solution under the influence of uniform and non-uniform electric fields (Liang *et al.*, 2014b). The case study with uniform electric field showed that the HS approximation agrees well with the CD solution at increasing solute concentration in a 2D unobstructed membrane channel. Their results found that the HS approximation is more accurate at higher solute mass fractions of 0.001 or more, which are the typical salt profiles encountered in RO desalination process. Hence, the HS forced-slip model is suitable for modelling the electro-osmotic effect in an RO membrane system.

19.5.4.3 Significant learnings of EOF slip velocity in CFD studies

The HS slip velocity model has been extensively validated and is suitable to be applied for the typical flow conditions encountered in real RO membrane modules (Liang *et al.*, 2014a; Liang *et al.*, 2014b, 2016b). It is reported that the EOF perturbation induced near the membrane surface results in the shedding of vortices in a 2D spacer-filled membrane channel, which tends to enhance fluid mixing and reduce concentration polarisation (as shown in Figure 14). In addition, the EOF induced vortex shedding also increases wall shear along the membrane that could potentially reduce the fouling tendency in the membrane system (Liang *et al.*, 2016a; Liang *et al.*, 2016b). The effectiveness of EOF slip velocity in enhancing membrane performance and the significant findings in CFD membrane studies are further elaborated in Table 3.

Table 3 Significant findings of application of electro-osmosis in membrane system

Membrane model	Reference	Main findings
2D unobstructed RO rectangular channel	Chan *et al*. (2020b)	A reduced-order model was developed for fast predictions of concentration polarisation in an RO membrane system under permeation condition.
2D unobstructed RO rectangular channel	Chan *et al*. (2020a)	A reduced-order model was proposed to study the effect of permeation in an RO membrane system with EOF slip velocity considered.
2D spacer-filled channel for RO SWM modules	Liang *et al*. (2016b)	First CFD study incorporating steady and unsteady EOF for enhancing mass transfer in 2D spacer-filled channels, using HS forced-slip approximation.
2D unobstructed RO membrane channel	Ratnayake *et al*. (2016)	A spatio-temporal frequency response analysis was performed to investigate the effect of waves of different frequencies for an EOF forced slip velocity and the impact of changes on solute concentration gradients.
2D spacer-filled channel for RO SWM modules	Liang *et al*. (2018a)	CFD study of non-sinusoidal waveforms of EOF slip velocity reported a similar membrane performance as those obtained by sinusoidal slip velocity, in terms of both mass transfer and wall shear.
2D spacer-filled RO membrane channel	Liang *et al*. (2020a)	A comparison study between forced slip velocity and oscillating feed perturbation found that both approaches predict similarly in terms of hydrodynamics and flux performance.
2D spacer-filled RO membrane channel	Foo *et al*. (2020)	CFD study of the effect of varying feed spacer geometries on membrane performance revealed that the resonant slip frequency increases as spacer size is increased due to stronger shear layer interactions. An increased in distance between spacers leads to a greater flux due to forced-slip, albeit the actual flux is smaller.
2D spacer-filled channel for RO SWM modules	Foo *et al*. (2021)	CFD study of varying spacer configurations found that the submerged configuration results in the largest flux increase under forced-slip effect at the expense of a relatively larger pressure drop.

19.5.4.4 Oscillating flow

Inducing oscillations in the bulk flow is an approach to enhance mass transfer in membrane systems by generating instabilities. Li *et al*. (1998) studied the use of oscillating inflow to promote vortex shedding at lower *Re* in microfiltration systems. Their results suggested that using a time-dependant inflow reduces the cake layer resistance and, therefore, increases the flux. CFD modelling was used by Liang *et al*. (2018b) to show that an oscillating inflow may promote vortex shedding increasing the magnitude of the flow velocity towards the membrane surface which was later validated by Liang *et al*. (2020b).

The oscillatory inflow (OI) approach is implemented in CFD by changing the inlet velocity from time-independent to time-dependant, giving place to a waveform. Sine and cosine functions are typically used as waveforms for OI, though, others like square and sawtooth waves are also possible to use. The sine waveform for OI is described by:

$$u_{osc} = u_{ave}\left[1 + A\sin(2\pi ft)\right] \qquad \text{Eq. 13}$$

where u_{osc} is the oscillatory inlet velocity (m s^{-1}), u_{ave} is the average inlet velocity, A is the oscillation normalised amplitude, f is the oscillation frequency (s^{-1}) and t is time (s). Figure 15 shows different waveforms previously used for the OI technique (plot as normalised velocity).

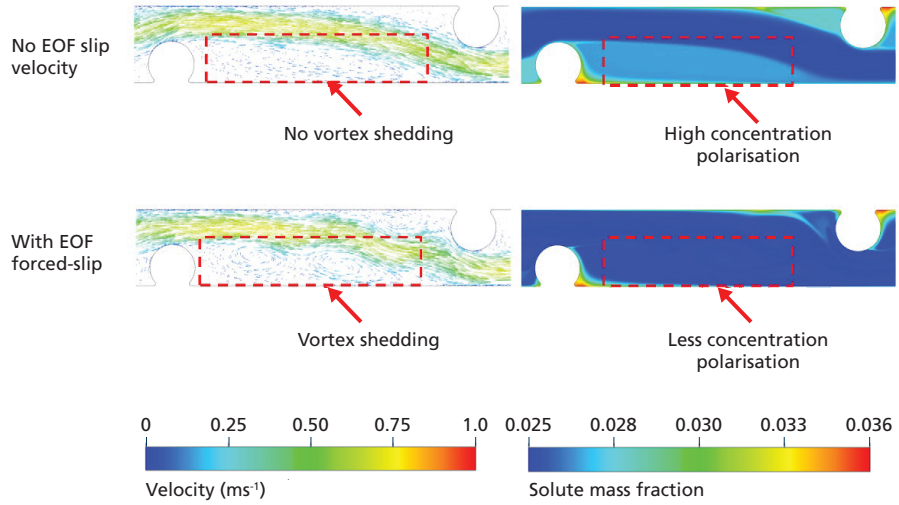

Figure 14 Effect of EOF slip velocity on velocity and solute concentration profiles in a unit cell of spacer-filled membrane channel (Foo *et al.*, 2020).

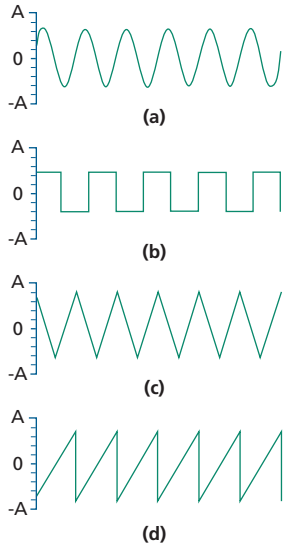

Figure 15 Waveforms for CFD analysis of OI technique: (a) sine, (b) square, (c) triangular and (d) sawtooth wave (Liang *et al.*, 2018b).

The optimal frequency of the oscillation to maximise mass transfer enhancement lies between 10 Hz and 1,000 Hz for typical spacer-filled membrane channels. A frequency response analysis can be used to identify the optimal response frequency for a membrane system. In a frequency response analysis, an input stimulus (commonly a short pulse) is introduced in the system and the response in velocity or concentration is recorded to find the maximum response. Recent approaches have undertaken the challenge of promoting vortex shedding at the minimum energy expenses by optimising the oscillating inflow amplitude and frequency.

19.5.4.5 Vibrations

Another approach to destabilise the boundary layer, instead of causing fluctuations in the flow, is to constantly move the module. Vibration-assisted modules use a mechanical device to induce oscillations on the channel enhancing mass transfer. Su *et al.* (2018) conducted a CFD study on concentration polarisation and permeate flux in a vibration enhanced system obtaining a reduction of up to 10% on the CP modulus when applying vibrations to the module. In addition, both the Sherwood number and permeate flux increased in about 15% and 5%, respectively, compared to the case without vibrations. In the same work, the results for permeate flux were validated experimentally. Studies on the effectiveness of vibration-assisted modules to mitigate CP are relatively recent and they are mainly focused on desalination processes (Li *et al.*, 2017; Su *et al.*, 2019). Thus, multiple aspects may be analysed to improve this technique such as optimal frequency and amplitude, waveform, etc.

19.5.5 Fouling modelling

Fouling phenomenon occurs in membranes due to solute deposited into the membrane pores or onto the surface. The phenomenon usually begins with a condition known as concentration polarisation (CP), which involves the solute accumulation near the membrane surface due to a greater applied pressure, compared to the osmotic pressure difference in the membrane process. There are two major types of fouling namely particulate fouling and biofouling phenomena. Particulate fouling occurs when foreign particles such as proteins, carbohydrates, oil, silt or clay are deposited into the membrane pores, leading to pore-blocking. The biofouling phenomenon, on the other hand, occurs due to the precipitation of microorganisms on the membrane surface, which leads to the formation of biofilm on the solid material. It is known that a prolonged fouling phenomenon would reduce the overall performance of a membrane module as permeate flux and membrane separation efficiency decrease (Fritzmann *et al.*, 2007).

19.5.5.1 Particulate fouling

Particulate fouling generally occurs when a solution containing particles with sizes ranging from few nanometres to micrometres dispersed evenly in the solution, eventually clogging the membrane pores. Particulate fouling condition can be reversed or becomes non-reversible depending on the types of foulant binding to the membrane surface. The phenomenon is said to be reversible if the particulate removal can be achieved via physical cleaning, and it is irreversible when foulant requires a chemical cleaning (Leam *et al.*, 2020). The particulates can be categorized into organic and inorganic substances, such that the organic particles are usually made up of proteins, carbohydrates, oils, etc., while the inorganic particles consist

of silt, clay, silica sediments, etc (Qasim *et al*., 2019). A continuous deposition of particles near the membrane surface over time results in the formation of a cake layer adjacent to the surface, which would impose a cake resistance onto the mass flow and eventually reduce the mass transport across the membrane, leading to a decrease in permeate flux (Jiang *et al*., 2017).

For the past few decades, CFD has been used to analyse the effects of particulate fouling on membrane performance as the software is capable of providing analysis for numerous flow and heat transfer mechanism, mass transport of soluble substrate, and the hydrodynamics of fluid flowing through the membrane for optimisation of membrane design through model simulations. A study on the particle deposition in a spiral wound membrane module was conducted to identify the optimum spacer type for preventing particulate fouling (Li *et al*., 2012). Flow that has lower velocity will lead to lower shear stress across membrane surface that promotes particulate fouling. Their study addressed the effects of curvature on the flow pattern for four different types of spacer configurations, namely zigzag, submerged, *i*-cavity, and *o*-cavity, respectively by changing the dimensionless radius of curvature, η given as follows:

$$\eta = \frac{R_o + R_i}{R_{ave}} \qquad \text{Eq. 14}$$

where R_o is the outer radius, R_i is the inner radius, and R_{ave} is their arithmetic mean (Li & Tung, 2008).

Based on the simulation results for empty channels and four spacer configurations of spacer-filled channels, a higher shear stress has the potential for a lower tendency for particle deposition as well as fouling. For submerged spacer-filled channels, it was found that the deposition ratio is greater at the outer membrane compared with that at the surface of the inner membrane. This can be explained by the lower shear stress observed at the surface of the outer membrane compared with that at the inner membrane due to a lower flow velocity near the outer membrane surface, which promotes the particulate fouling at the outer membrane surface. An illustration that depicts the deposition ratio at different positions of membrane in the submerged spacer-filled channels is shown in Figure 16.

In the case of asymmetric spacer-filled channels, it is reported that curve channels result in a higher particulate deposition ratio at the outer membrane surface compared with that of the flat channel because of a lower shear stress. This occurs because the curve channel tends to direct the fluid flow into the inner membrane surface, which restrains the recirculation size and decreases the velocity near the inner surface of the membrane. A summary on the significant findings of particulate fouling in membrane studies by CFD is listed in Table 4.

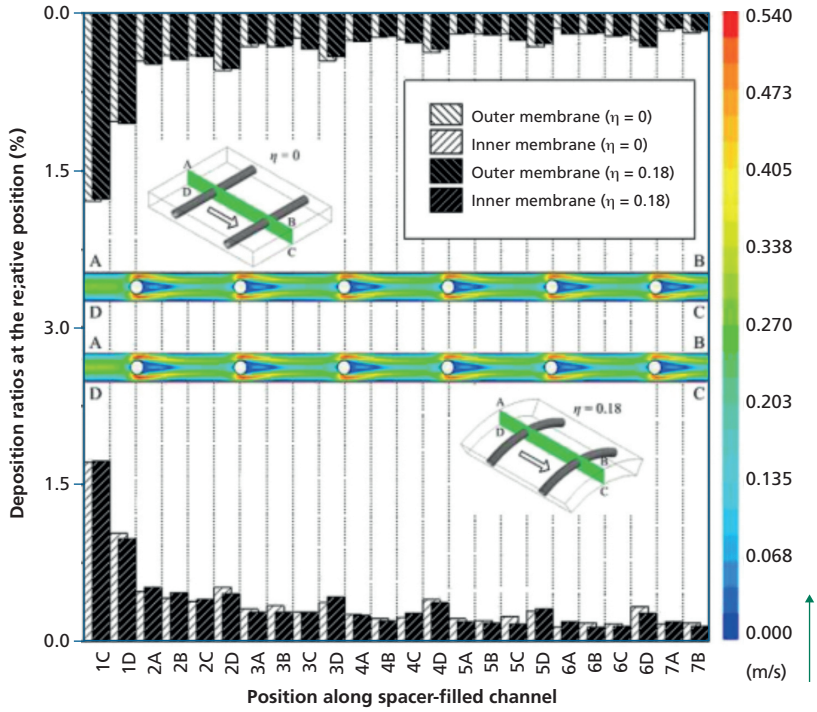

Figure 16 The deposition ratios on the inner and outer membranes in the flat and curved channel filled with submerged spacers at various positions (Li *et al.*, 2012).

Table 4 Significant findings of CFD studies on particulate fouling in membranes

Author	Research types	Main findings	Observations
Lin *et al.* (2022a)	CFD and Response surface methodology (RSM)	Diagonal-flow feed channel results in a higher salt rejection and water flux with an average crossflow velocity in the channel increased by ~50%, compared to that in the conventional feed channel.	The study is limited to feed channels without considering the effects of feed spacer.
Rahimi *et al.* (2009)	CFD and experimental	Fouling on membrane is not uniform and the possibilities of fouling to happen are higher in regions with lower shear stress.	The study is limited to an incompressible flow system.
Li *et al.* (2012)	CFD only	Recirculation occurred adjacent to the membrane and behind the filament causing a higher shear stress, which potentially reduces particulate fouling in the membrane system.	This study is limited to a low volume fraction of discrete phase that ranges less than 10-12%. It is also limited to a two-phase flow.

19.5.5.2 Tracer test

Tracer test or commonly known as the Salt Tracer Response Technique (STRT), is frequently used to evaluate the effects of cake-enhanced osmotic pressure (CEOP) on the development of concentration polarisation in a membrane system. It is reported that a larger extent of CEOP indicates an elevated solute concentration near the membrane surface due to the formation of a cake-layer, which obstructs the back-diffusion of solute into the bulk solution (Taheri *et al.*, 2015). This eventually causes an increase in the transmembrane pressure (TMP), in which more energy is required to push the fluid through the membrane.

CFD technique is used to assess and interpret the results from tracer test for estimating the fouling resistance and concentration polarisation. A study conducted by Fimbres Weihs & Wiley (2014) focuses on the effect of cake-enhanced osmotic pressure on particulate fouling. The tracer test technique is used to monitor the TMP, permeate flux, and solute concentration in the permeate by injecting sodium chloride as the tracer into the feed stream of a membrane separation unit (Chong *et al.*, 2007). A *CP* index is used to measure the extent of *CP*, which can be defined in a one-dimensional mass balance differential equation, given as follows:

$$CP = \frac{w_w - w_p}{w_b - w_p} = \exp\left(\frac{J_v}{k_{mt}}\right) \qquad \text{Eq. 15}$$

where *CP* is the local *CP* index based on local solute bulk concentration, k_{mt} is the mass transfer coefficient, and J_v is the volumetric permeate flux.

Results from the tracer test found that a step change in feed concentration does not affect the degree of concentration polarisation across the membrane. The *CP* index was found to be over-estimated, which can be explained by the entrance effects limited by spacers, such that the presence of spacers separating the membrane leaves would eventually shift the velocity profile of fluid towards the module inlet. The over-estimation in the fouled membrane is greater and the overestimation of *CP* index decreases with higher tracer concentration but increases with fouling layer mass, which reduces the membrane performance in terms of reducing particulate fouling. However, it is important to make assumptions to maintain a constant CPM index to identify precise error results on constant pressure tracer response tests because changing salt concentration may alter the specific cake resistance that will lead to deviation in over-estimation.

19.5.5.3 Biofouling

Biofouling phenomena occur due to the accumulation and adhesion of microorganisms on the membrane surface, leading to the formation of a biofilm on the membrane. The biofilm layer is commonly composed of an extracellular polymeric substance (EPS) matrix, which is a polymer-like material enclosed with microorganisms on the surface (Unal, 2022). The extent of biofouling can depend on several factors such as membrane characteristics, influent composition and microorganism types. Most biofouling instances occur as a result

of a symbiotic interaction between bacteria, algae and fungus. Another fact to consider when dealing with biofouling, is that a significant amount of the cells attached to the membrane are dead cells, meaning that biofouling leads to organic fouling. Recent advances on membrane science have focused on producing membranes with high surface hydrophobicity and low surface roughness, as it has been found that membranes with these characteristics have a lower tendency for biofouling, due to smaller exposed areas and less active sites for microbial adhesion (Maddah & Chogle, 2016). Furthermore, the development of a biofilm depends, in general, on the substrate availability and the type of microorganisms on the feed stream.

A recent study by Lin *et al.* (2022b) numerically and experimentally investigated the effects of feed spacer geometries and channel porosity on the degree of biofouling in the membrane system. Feed spacer geometries were varied in terms of the filament length, diameter, mesh angle, as well as spacer thickness to obtain different channel porosities. The porosity of the feed spacer membrane channel is calculated using the following equation:

$$\delta_{channel} = 1 - \frac{V_{spacer}}{V_{channel}} = 1 - \frac{\left(\frac{\pi}{4}D^2\right)L}{HL^2 \sin\alpha} = 1 - \frac{\pi D^2}{2HL\sin\alpha} \quad \text{Eq. 16}$$

where D is filament diameter (m), L is filament length (m), H is spacer thickness (m), and α is mesh angle. The channel porosity is an important factor in determining the feed channel pressure (FCP) drop. A larger channel porosity will generally result in less FCP drop, as there are less flow obstructions per unit of channel volume. Furthermore, larger porosity also generally leads to less biomass accumulation, due to less stagnant flow regions and larger shear.

Lin *et al.* (2022b) noted that several experimental studies report that higher shear stress conditions tend to promote biofouling because of a higher nutrient load enhances biomass accumulation, although the biofilm forming on high shear stress regions would be thinner and more compacted. In addition, their analysis shows that the average cross-flow velocity decreases with increasing filament length and spacer thickness due to reduced turbulence caused by the number of spacer filament per unit channel length and the increment of space between spacer filament and membrane surface, respectively. However, the average velocity increases at a larger mesh angle or larger filament diameter. This is because a decrease in the distance between the neighbouring spacer meshes and a narrow space between the spacer filament and the membrane surface cause more turbulence in the fluid flow. It was also found that an increase in the filament diameter and/or a decrease in the spacer thickness promotes the accumulation of biomass, which favours the growth of bacteria on the membrane surface as the interspace between the membrane and spacer filaments is reduced. Therefore, a thicker feed spacer is recommended as higher feed channel porosity tends to reduce biofouling in the membrane system (Bucs *et al.*, 2014). A summary of significant findings related to biofouling in membrane systems by CFD is presented in Table 5.

Table 5 Significant findings of CFD studies on biofouling in membrane system

References	Research types	Main findings	Observations
Vrouwenvelder *et al*. (2010)	CFD only	The presence of spacer strongly affects the level of pressure drop as an increment of 10 times the pressure drop in the feed channel is reported, when compared with the experimental case without spacer. Fouling on the feed spacer is more important than fouling on the membrane.	This study is limited to one spacer geometry, specifically on the spacer thickness of 31 mil.
Gu *et al*. (2017)	CFD only	Fully woven spacers result in the highest water flux and have lower average concentration polarisation moduli.	The study is limited to hydrodynamics and ignores mass transfer along the channel.
Li *et al*. (2016)	CFD only	Regions with high concentration of biomass are isolated to zones near the spacer filaments in which the flow is relatively static. The fouling tendencies are higher in the stagnant regions because the particles can settle down more easily.	The study is limited to one type of spacer geometry without considering the effects of spacer geometry on CP.
Chen and Wu (2021)	CFD only	A larger average pore size of the membrane increases the nucleation frequency and growth rate of membrane biofouling. At lower velocity, the flow rate decreases more than 50%, partly contributed by the decreased low permeate flux caused by fouling.	This study lacks focus on the effects of pressure drop in determining the degree of concentration polarisation.

An approach to model biofouling development and its effect on mass transfer in membrane systems is to consider the biofilm as a different phase. The biofilm phase is considered to have different mass transfer properties for the models. The solute concentration and the biofilm are linked by introducing a mathematical model to describe the biomass growth as a function of the substrate concentration. The Monod equation is possibly the simplest model to describe the cell growth rate in terms of the substrate concentration. This differential equation states that the cell growth rate is directly proportional to the number of cells, but limited by the substrate availability. The Monod equation is described as:

$$\frac{dC_X}{dt} = \mu_{\max} \frac{C_S}{K_S + C_S} C_X \qquad \text{Eq. 17}$$

where C_X is the biomass concentration (kg m^{-3}), μ_{max} is maximum growth rate (s^{-1}), C_S (kgm^{-3}) is the substrate concentration and K_S is the half-velocity constant (kg m^{-3}).

More sophisticated models may take into account the cell growth phase, the inhibitory effect of the components of the media (e.g., sodium chloride, chlorine, reactive oxygen species, etc.). Radu *et al*. (2010) conducted a numerical study on the biofilm formation in

a spacer-filled membrane channel coupling COMSOL and MATLAB. Figure 17 shows a graphic overview of the process for biofouling modelling used by Radu *et al.* (2010). The biomass growth rate is modelled using Monod equation with a random seeding on the filament wall or membrane surface. A finite element mesh is used to discretise the fluid and the biofilm sub-domains. The hydrodynamics, solute concentration and substrate concentration are solved via CFD. The biofilm growth is modelled according to the substrate distribution and then updated into the CFD model. Finally, an attachment/detachment step is added based on the mechanical stress. This process is repeated for each timestep to follow the time evolution of the biofilms.

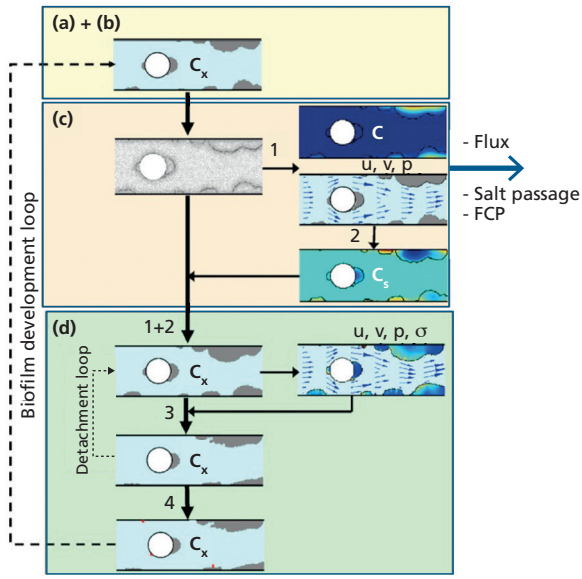

Figure 17 Adaptive algorithm for modelling of biofilm evolution using a hybrid CFD/numerical approach (Radu *et al.*, 2010).

19.6 ADDITIONAL CONSIDERATIONS

19.6.1 Multi-scale modelling

Despite of being a powerful tool for analysis, CFD studies typically focus only on a small-scale model in order to facilitate the modelling of an MSP. Multi-scale modelling refers to the analysis of fluids at different scales of space and/or time (Steinhauser, 2017). While analysing the operational advantages of a certain technique in a small-scale model may be useful to determine its effectivity, in some cases, it is worth to analyse the large-scale effects as they are directly linked to the feasibility of the approach. For example, using an instantaneous pulse as the inflow for a membrane system may enhance mass transfer over a short period of time, but this effect is negligible compared to the large operation periods of actual systems. Indicators such as pressure drop and permeate flux can be used to extrapolate

the efficiency of a full-length membrane system. Furthermore, optimising the separation performance of the system can lead to energy savings during operation; although, these may be negligible when compared to the energy requirements of the whole process.

19.6.1.1 Techno-economics

Techno-economic analyses are used to determine the cost-effectiveness of a process or a modification made to it, by estimating the overall production cost of the product (Toh *et al.*, 2020a). A unitary cost per volume (e.g., dollars per m^3) is used to reflect the processing cost for producing treated water. A comprehensive techno-economic analysis would include both capital and operational costs which are difficult to determine as they depend on geographical and time factors (Toh *et al.*, 2020a). The results obtained via CFD analysis are useful to carry out a simplified techno-economic assessment considering only operational costs related to the membrane operation such as pre-treatment, operating pressure, pressure drop and permeate flux (Liang *et al.*, 2019).

19.7 OUTLOOK

Instead of focusing on the spacer geometry, recent CFD studies on membrane systems are focusing on new strategies to promote transient laminar flow and induce vortex shedding such as unsteady inflow, vibration-assisted modules and electroosmosis. In addition, the number of studies including experimental validation is increasing due to the necessity of assessing the feasibility for real-life applications. At the time, there is a gap between CFD studies and real-life applications which demands for more effective ways to scale-up the models. Comprehensive techno-economic studies are increasingly being included to assess the economic benefits of implementing a new technique.

Over the last decade, 2D CFD models are becoming sparse due to the increasing capability of modern computers that significantly reduced the computational time required for 3D simulations. The soaring development of new technology allows higher resolution with less computational time and has introduced new approaches for data analysis. New studies including advanced modelling techniques are frequently appearing in an effort to extract the most information from CFD analysis. This modelling techniques include tools like big data, machine learning and reduced-order modelling. The arrival of techniques such as micro- and holographic-particle image velocimetry is allowing the validation of micro-scale phenomena studied by CFD during the recent years.

19.8 REFERENCES

Ahmad, A. L., Lau, K. K., Bakar, M. A., & Shukor, S. A. (2005). Integrated CFD simulation of concentration polarization in narrow membrane channel. Computers & Chemical Engineering, 29(10), 2087-2095. doi:https://doi.org/10.1016/j.compchemeng.2005.06.001

Alexiadis, A., Wiley, D., Fletcher, D., & Bao, J. (2007). Laminar flow transitions in a 2D channel with circular spacers. Industrial & Engineering Chemistry Research, 46(16), 5387-5396. doi:https://doi.org/10.1021/ie0607797

Anderson, J. D., & Wendt, J. (1995). Computational fluid dynamics (Vol. 206): Springer.

Anderson, J. L. (1989). Colloid transport by interfacial forces. Annual review of fluid Mechanics, 21(1), 61-99.

ANSYS Inc. (2012). ANSYS CFX Solver theory guide. Canonsburg.

ANSYS Inc. (2020). ANSYS Fluent Users Guide. Canonsburg.

ANSYS Inc. (2021). ANSYS CFX Solver Manager User's Guide. Canonsburg.

Antony, A., Chilcott, T., Coster, H., & Leslie, G. (2013). In situ structural and functional characterization of reverse osmosis membranes using electrical impedance spectroscopy. Journal of Membrane science, 425-426, 89-97. doi:https://doi.org/10.1016/j.memsci.2012.09.028

Asadi, A., Huat, B. B., Nahazanan, H., & Keykhah, H. A. (2013). Theory of electroosmosis in soil. International Journal of Electrochemical Science, 8(1), 1016-1025.

Asefi, H., Alighardashi, A., Fazeli, M., & Fouladitajar, A. (2019). CFD modeling and simulation of concentration polarization reduction by gas sparging cross-flow nanofiltration. Journal of Environmental Chemical Engineering, 7(5), 103275. doi:https://doi.org/10.1016/j.jece.20r19.103275

Baghel, R., Kalla, S., Upadhyaya, S., Chaurasia, S., & Singh, K. (2020). CFD modeling of vacuum membrane distillation for removal of Naphthol blue black dye from aqueous solution using COMSOL multiphysics. Chemical Engineering Research and Design, 158, 77-88. doi:https://doi.org/10.1016/j.cherd.2020.03.016

Baker, R. W. (2004). Membrane Technology and Applications. England: John Wiley & Sons Ltd.

Baker, R. W. (2012). Membrane technology and applications: John Wiley & Sons.

Balster, J. (2016). Hollow Fiber Membrane Module. In E. Drioli & L. Giorno (Eds.), Encyclopedia of Membranes (pp. 955-957). Berlin, Heidelberg: Springer Berlin Heidelberg.

Behroozi, A. H., Kasiri, N., & Mohammadi, T. (2019). Multi-phenomenal macroscopic investigation of cross-flow membrane flux in microfiltration of oil-in-water emulsion, experimental & computational. Journal of Water Process Engineering, 32, 100962. doi:https://doi.org/10.1016/j.jwpe.2019.100962

Berk, Z. (2009). Chapter 10 - Membrane processes. In Z. Berk (Ed.), Food Process Engineering and Technology (pp. 233-257). San Diego: Academic Press.

Boussu, K., Van der Bruggen, B., Volodin, A., Snauwaert, J., Van Haesendonck, C., & Vandecasteele, C. (2005). Roughness and hydrophobicity studies of nanofiltration membranes using different modes of AFM. Journal of colloid and interface science, 286(2), 632-638. doi:https://doi.org/10.1016/j.jcis.2005.01.095

Brunner, D., Khawaja, H., Moatamedi, M., & Boiger, G. (2018). CFD modelling of pressure and shear rate in torsionally vibrating structures using ANSYS CFX and COMSOL Multiphysics. The International Journal of Multiphysics, 12(4), 349-358. doi:https://doi.org/10.21152/1750-9548.12.4.349

Bucs, S. S., Valladares Linares, R., van Loosdrecht, M. C., Kruithof, J. C., & Vrouwenvelder, J. S. (2014). Impact of organic nutrient load on biomass accumulation, feed channel pressure drop increase and permeate flux decline in membrane systems. Water Res, 67, 227-242. doi:10.1016/j.watres.2014.09.005

Burn, S., & Gray, S. (2015). Efficient Desalination by Reverse Osmosis: A guide to RO practice (Vol. 14). London, UK: IWA Publishing.

Byun, H. S., & Rhee, K. (2004). CFD modeling of blood flow following coil embolization of aneurysms. Medical engineering & physics, 26(9), 755-761. doi:https://doi.org/10.1016/j.medengphy.2004.06.008

Cancilla, N., Gurreri, L., Marotta, G., Ciofalo, M., Cipollina, A., Tamburini, A., & Micale, G. (2021). CFD prediction of shell-side flow and mass transfer in regular fiber arrays. International Journal of Heat and Mass Transfer, 168, 120855. doi:https://doi.org/10.1016/j.ijheatmasstransfer.2020.120855

Cao, Z., Wiley, D., & Fane, A. (2001). CFD simulations of net-type turbulence promoters in a narrow channel. Journal of Membrane science, 185(2), 157-176. doi:https://doi.org/10.1016/s0376-7388(00)00643-8

Chan, F. S., Tan, C. K., Ratnayake, P., Junaidi, M. U. M., & Liang, Y. Y. (2020a). Reduced-order modelling of concentration polarization with varying permeation: Analysis of electro-osmosis in membranes. Desalination, 495, 114677. doi:https://doi.org/10.1016/j.desal.2020.114677

Chan, F. S., Tan, C. K., Ratnayake, P., & Liang, Y. Y. (2020b). Reduced-order modeling of flow and concentration polarization in membrane systems with permeation. AIChE journal, 66(4), e16851. doi:https://doi.org/10.1002/aic.16851

Chen, L., & Wu, B. (2021). Research Progress in Computational Fluid Dynamics Simulations of Membrane Distillation Processes: A Review. Membranes (Basel), 11(7). doi:10.3390/membranes11070513

Chong, T. H., Wong, F. S., & Fane, A. G. (2007). Enhanced concentration polarization by unstirred fouling layers in reverse osmosis: Detection by sodium chloride tracer response technique. Journal of Membrane science, 287(2), 198-210. doi:10.1016/j.memsci.2006.10.035

Chong, Y. K., Liang, Y. Y., Lau, W. J., & Fimbres Weihs, G. A. (2022). 3D CFD study of hydrodynamics and mass transfer phenomena for spiral wound membrane submerged-type feed spacer with different node geometries and sizes. International Journal of Heat and Mass Transfer, 191, 122819. doi:https://doi.org/10.1016/j.ijheatmasstransfer.2022.122819

Chu, A., Kwok, R. C.-W., & Yu, K. (2005). Study of pollution dispersion in urban areas using Computational Fluid Dynamics (CFD) and Geographic Information System (GIS). Environmental Modelling & Software, 20(3), 273-277. doi:https://doi.org/10.1016/j.envsoft.2004.05.007

COMSOL AB. (2008). COMSOL Multiphysics User's Guide. Burlington.

Cummings, E. B., Griffiths, S. K., Nilson, R. H., & Paul, P. H. (2000). Conditions for Similitude between the Fluid Velocity and Electric Field in Electroosmotic Flow. Analytical Chemistry, 72(11), 2526-2532. doi:10.1021/ac991165x

Da Costa, A., Fane, A., & Wiley, D. (1994). Spacer characterization and pressure drop modelling in spacer-filled channels for ultrafiltration. Journal of Membrane science, 87(1-2), 79-98. doi:https://doi.org/10.1016/0376-7388(93)e0076-p

Du, X., Liu, X., Wang, Y., Radaei, E., Lian, B., Leslie, G., Li, G., & Liang, H. (2017). Particle deposition on flat sheet membranes under bubbly and slug flow aeration in coagulation-microfiltration process: Effects of particle characteristic and shear stress. Journal of Membrane science, 541, 668-676. doi:https://doi.org/10.1016/j.memsci.2017.07.023

Fimbres-Weihs, G., & Wiley, D. (2008). Numerical study of two-dimensional multi-layer spacer designs for minimum drag and maximum mass transfer. Journal of Membrane science, 325(2), 809-822. doi:https://doi.org/10.1016/j.memsci.2008.09.005

Fimbres-Weihs, G., & Wiley, D. (2010). Review of 3D CFD modeling of flow and mass transfer in narrow spacer-filled channels in membrane modules. Chemical Engineering and Processing: Process Intensification, 49(7), 759-781. doi:https://doi.org/10.1016/j.cep.2010.01.007

Fimbres-Weihs, G. A., Wiley, D. E., & Fletcher, D. F. (2006). Unsteady Flows with Mass Transfer in Narrow Zigzag Spacer-Filled Channels: A Numerical Study. Industrial & Engineering Chemistry Research, 45(19), 6594-6603. doi:10.1021/ie060243l

Fimbres Weihs, G., & Wiley, D. (2007). Numerical study of mass transfer in three-dimensional spacer-filled narrow channels with steady flow. Journal of Membrane science, 306, 228-243. doi:10.1016/j.memsci.2007.08.043

Fimbres Weihs, G. A., & Wiley, D. E. (2014). CFD analysis of tracer response technique under cake-enhanced osmotic pressure. Journal of Membrane science, 449, 38-49. doi:10.1016/j.memsci.2013.08.015

Foo, K., Liang, Y. Y., & Fimbres Weihs, G. A. (2020). CFD study of the effect of SWM feed spacer geometry on mass transfer enhancement driven by forced transient slip velocity. Journal of Membrane science, 597. doi:10.1016/j.memsci.2019.117643

Foo, K., Liang, Y. Y., Tan, C. K., & Fimbres Weihs, G. A. (2021). Coupled effects of circular and elliptical feed spacers under forced-slip on viscous dissipation and mass transfer enhancement based on CFD. Journal of Membrane science, 637, 119599. doi:https://doi.org/10.1016/j.memsci.2021.119599

Fritzmann, C., Löwenberg, J., Wintgens, T., & Melin, T. (2007). State-of-the-art of reverse osmosis desalination. Desalination, 216(1-3), 1-76. doi:10.1016/j.desal.2006.12.009

Gavelli, F., Bullister, E., & Kytomaa, H. (2008). Application of CFD (Fluent) to LNG spills into geometrically complex environments. Journal of hazardous materials, 159(1), 158-168. doi:https://doi.org/10.1016/j.jhazmat.2008.02.037

Geraldes, V., & Afonso, M. D. (2006). Generalized mass- transfer correction factor for nanofiltration and reverse osmosis. AIChE journal, 52(10), 3353-3362. doi:https://doi.org/10.1002/aic.10968

Golrokh Sani, A., Najafi, H., & Azimi, S. S. (2021). CFD simulation of air-sparged slug flow in the flat-sheet membrane: A concentration polarization study. Separation and Purification Technology, 270, 118816. doi:https://doi.org/10.1016/j.seppur.2021.118816

Gu, B., Adjiman, C. S., & Xu, X. Y. (2017). The effect of feed spacer geometry on membrane performance and concentration polarisation based on 3D CFD simulations. Journal of Membrane science, 527, 78-91. doi:https://doi.org/10.1016/j.memsci.2016.12.058

Gupta, R., Fletcher, D. F., & Haynes, B. S. (2009). On the CFD modelling of Taylor flow in microchannels. Chemical Engineering Science, 64(12), 2941-2950. doi:https://doi.org/10.1016/j.ces.2009.03.018

Haddadi, B., Jordan, C., Miltner, M., & Harasek, M. (2018). Membrane modeling using CFD: Combined evaluation of mass transfer and geometrical influences in 1D and 3D. Journal of Membrane science, 563, 199-209. doi:https://doi.org/10.1016/j.memsci.2018.05.040

Hinsch, K. D. (2002). Holographic particle image velocimetry. Measurement Science and Technology, 13(7), R61-R72. doi:10.1088/0957-0233/13/7/201

Holemans, T., Yang, Z., & Vanierschot, M. (2022). Efficient Reduced Order Modeling of Large Data Sets Obtained from CFD Simulations. Fluids, 7(3), 110. doi:https://doi.org/10.3390/fluids7030110

Hu, G., & Li, D. (2007). Multiscale phenomena in microfluidics and nanofluidics. Chemical Engineering Science, 62(13), 3443-3454. doi:https://doi.org/10.1016/j.ces.2006.11.058

Hunter, R. J. (2013). Zeta potential in colloid science: principles and applications (Vol. 2): Academic press.

Jafarkhani, M., Moraveji, M. K., Davarnejad, R., Moztarzadeh, F., & Mozafari, M. (2012). Three-dimensional simulation of turbulent flow in a membrane tube filled with semi-circular baffles. Desalination, 294, 8-16. doi:https://doi.org/10.1016/j.desal.2012.02.031

Jagannadh, S. N., & Muralidhara, H. S. (1996). Electrokinetics Methods To Control Membrane Fouling. Industrial & Engineering Chemistry Research, 35(4), 1133-1140. doi:10.1021/ie9503712

Jamshed, S. (2015). Using HPC for Computational Fluid Dynamics: A Guide to High Performance Computing for CFD Engineers: Academic Press.

Javid, S. M., Passandideh-Fard, M., Faezian, A., & Goharimanesh, M. (2017). Slug and bubble flows in a flat sheet ultrafiltration module: Experiments and numerical simulation. International Journal of Multiphase Flow, 91, 39-50. doi:https://doi.org/10.1016/j.ijmultiphaseflow.2016.12.006

Jiang, S., Li, Y., & Ladewig, B. P. (2017). A review of reverse osmosis membrane fouling and control strategies. Sci Total Environ, 595, 567-583. doi:10.1016/j.scitotenv.2017.03.235

Junker, M. A., de Vos, W. M., Lammertink, R. G. H., & de Grooth, J. (2021). Bridging the gap between lab-scale and commercial dimensions of hollow fiber nanofiltration membranes. Journal of Membrane science, 624, 119100. doi:https://doi.org/10.1016/j.memsci.2021.119100

Kaya, R., Deveci, G., Turken, T., Sengur, R., Guclu, S., Koseoglu-Imer, D. Y., & Koyuncu, I. (2014). Analysis of wall shear stress on the outside-in type hollow fiber membrane modules by CFD simulation. Desalination, 351, 109-119. doi:https://doi.org/10.1016/j.desal.2014.07.033

Kone, J.-P., Zhang, X., Yan, Y., Hu, G., & Ahmadi, G. (2018). CFD modeling and simulation of PEM fuel cell using OpenFOAM. Energy Procedia, 145, 64-69. doi:https://doi.org/10.1016/j.egypro.2018.04.011

Landahl, M. T., Mollo- Christensen, E., & Korman, M. S. (1989). Turbulence and random processes in fluid mechanics. In: Acoustical Society of America.

Leam, J. J., Bilad, M. R., Wibisono, Y., Hakim Wirzal, M. D., & Ahmed, I. (2020). Membrane Technology for Microalgae Harvesting. 97-110. doi:10.1016/b978-0-12-817536-1.00007-2

Li, H. y., Bertram, C. D., & Wiley, D. E. (1998). Mechanisms by which pulsatile flow affects cross-flow microfiltration. AIChE journal, 44(9), 1950-1961. doi:https://doi.org/10.1002/aic.690440903

Li, M., Bui, T., & Chao, S. (2016). Three-dimensional CFD analysis of hydrodynamics and concentration polarization in an industrial RO feed channel. Desalination, 397, 194-204. doi:https://doi.org/10.1016/j.desal.2016.07.005

Li, W., Su, X., Palazzolo, A., Ahmed, S., & Thomas, E. (2017). Reverse osmosis membrane, seawater desalination with vibration assisted reduced inorganic fouling. Desalination, 417, 102-114. doi:. https://doi.org/10.1016/j.desal.2017.05.016

Li, Y.-L., & Tung, K.-L. (2008). The effect of curvature of a spacer-filled channel on fluid flow in spiral-wound membrane modules. Journal of Membrane science, 319(1-2), 286-297. doi:10.1016/j.memsci.2008.03.069

Li, Y.-L., Tung, K.-L., Chen, Y.-S., & Hwang, K.-J. (2012). CFD analysis of the initial stages of particle deposition in spiral-wound membrane modules. Desalination, 287, 200-208. doi:10.1016/j.desal.2011.10.001

Liang, Y. Y., Chapman, M. B., Fimbres-Weihs, G. A., & Wiley, D. E. (2014a). CFD modelling of electro-osmotic permeate flux enhancement on the feed side of a membrane module. Journal of Membrane science, 470, 378-388. doi:https://doi.org/10.1016/j.memsci.2014.07.039

Liang, Y. Y., Fimbres-Weihs, G. A., & Fletcher, D. F. (2018a). CFD study of the effect of unsteady slip velocity waveform on shear stress in membrane systems. Chemical Engineering Science, 192, 16-24. doi:https://doi.org/10.1016/j.ces.2018.07.009

Liang, Y. Y., Fimbres-Weihs, G. A., Setiawan, R., & Wiley, D. E. (2016a). CFD modelling of unsteady electro-osmotic permeate flux enhancement in membrane systems. Chemical Engineering Science, 146, 189-198. doi:https://doi.org/10.1016/j.ces.2016.02.028

Liang, Y. Y., Fimbres-Weihs, G. A., & Wiley, D. E. (2014b). Approximation for modelling electro-osmotic mixing in the boundary layer of membrane systems. Journal of Membrane science, 450, 18-27. doi:https://doi.org/10.1016/j.memsci.2013.08.031

Liang, Y. Y., Fimbres-Weihs, G. A., & Wiley, D. E. (2016b). CFD modelling of electro-osmotic permeate flux enhancement in spacer-filled membrane channels. Journal of Membrane science, 507, 107-118. doi:https://doi.org/10.1016/j.memsci.2016.02.012

Liang, Y. Y., Fimbres-Weihs, G. A., & Wiley, D. E. (2020a). Comparison of oscillating flow and slip velocity mass transfer enhancement in spacer-filled membrane channels: CFD analysis and validation. Journal of Membrane science, 593, 117433. doi:https://doi.org/10.1016/j.memsci.2019.117433

Liang, Y. Y., Fimbres Weihs, G. A., & Fletcher, D. F. (2018b). CFD study of the effect of unsteady slip velocity waveform on shear stress in membrane systems. Chemical Engineering Science, 192, 16-24. doi:https://doi.org/10.1016/j.ces.2018.07.009

Liang, Y. Y., Fimbres Weihs, G. A., & Wiley, D. E. (2020b). Comparison of oscillating flow and slip velocity mass transfer enhancement in spacer-filled membrane channels: CFD analysis and validation. Journal of Membrane science, 593, 117433. doi:https://doi.org/10.1016/j.memsci.2019.117433

Liang, Y. Y., Toh, K. Y., & Fimbres Weihs, G. A. (2019). 3D CFD study of the effect of multi-layer spacers on membrane performance under steady flow. Journal of Membrane science, 580, 256-267. doi:https://doi.org/10.1016/j.memsci.2019.02.015

Lin, W., Lei, J., Wang, Q., Wang, X.-m., & Huang, X. (2022a). Performance enhancement of spiral-wound reverse osmosis membrane elements with novel diagonal-flow feed channels. Desalination, 523, 115447.

Lin, W., Wang, Q., Sun, L., Wang, D., Cabrera, J., Li, D., Hu, L., Jiang, G., Wang, X.-m., & Huang, X. (2022b). The critical role of feed spacer channel porosity in membrane biofouling: Insights and implications. Journal of Membrane science, 649, 120395.

Lindken, R., & Burgmann, S. (2012). 14 - Laser-optical methods for transport studies in low temperature fuel cells. In C. Hartnig & C. Roth (Eds.), Polymer Electrolyte Membrane and Direct Methanol Fuel Cell Technology (Vol. 2, pp. 425-461): Woodhead Publishing.

Liu, D., Bu, C., & Chen, X. (2013). Development and test of CFD–DEM model for complex geometry: A coupling algorithm for Fluent and DEM. Computers & Chemical Engineering, 58, 260-268. doi:https://doi.org/10.1016/j.compchemeng.2013.07.006

Liu, Y., & Hinrichsen, O. (2014). CFD modeling of bubbling fluidized beds using OpenFOAM®: Model validation and comparison of TVD differencing schemes. Computers & Chemical Engineering, 69, 75-88. doi:https://doi.org/10.1016/j.compchemeng.2014.07.002

Lotfiyan, H., Zokaee Ashtiani, F., Fouladitajar, A., & Armand, S. B. (2014). Computational fluid dynamics modeling and experimental studies of oil-in-water emulsion microfiltration in a flat

sheet membrane using Eulerian approach. Journal of Membrane science, 472, 1-9. doi:https://doi.org/10.1016/j.memsci.2014.08.036

Maddah, H., & Chogle, A. (2016). Biofouling in reverse osmosis: phenomena, monitoring, controlling and remediation. Applied Water Science, 7(6), 2637-2651. doi:10.1007/s13201-016-0493-1

Martín, M. M. (2016). Chapter 4 - Water. In M. M. Martín (Ed.), Industrial Chemical Process Analysis and Design (pp. 125-197). Boston: Elsevier.

Martinelli, L., Guigui, C., & Line, A. (2010). Characterisation of hydrodynamics induced by air injection related to membrane fouling behaviour. Desalination, 250(2), 587-591. doi:https://doi.org/10.1016/j.desal.2009.09.029

NASA. (2022). Overview of CFD Verification & Validation. Retrieved from https://www.grc.nasa.gov/www/wind/valid/tutorial/overview.html

Ndinisa, N. V., Wiley, D. E., & Fletcher, D. F. (2005). Computational Fluid Dynamics Simulations of Taylor Bubbles in Tubular Membranes: Model Validation and Application to Laminar Flow Systems. Chemical Engineering Research and Design, 83(1), 40-49. doi:https://doi.org/10.1205/cherd.03394

OpenCFD Ltd. (2016). OpenFOAM: User Guide. Retrieved from https://www.openfoam.com/documentation/guides/latest/doc/guide-schemes.html

Ouyang, H., Bao, J., Fimbres-Weihs, G. A., & Wiley, D. E. (2013). Control study on mixing enhancement in boundary layers of membrane systems. Journal of Process Control, 23(8), 1197-1204. doi:https://doi.org/10.1016/j.jprocont.2013.07.005

Pak, A., Mohammadi, T., Hosseinalipour, S. M., & Allahdini, V. (2008). CFD modeling of porous membranes. Desalination, 222(1), 482-488. doi:https://doi.org/10.1016/j.desal.2007.01.152

Park, S., Jeong, Y. D., Lee, J. H., Kim, J., Jeong, K., & Cho, K. H. (2021). 3D printed honeycomb-shaped feed channel spacer for membrane fouling mitigation in nanofiltration. Journal of Membrane science, 620, 118665. doi:https://doi.org/10.1016/j.memsci.2020.118665

Patankar, N. A., & Hu, H. H. (1998). Numerical Simulation of Electroosmotic Flow. Analytical Chemistry, 70(9), 1870-1881. doi:10.1021/ac970846u

Probstein, R. F. (1989). Physiochemical Hydrodynamics: An Introduction. Hoboken, New Jersey: John Wiley & Sons.

Qasim, M., Badrelzaman, M., Darwish, N. N., Darwish, N. A., & Hilal, N. (2019). Reverse osmosis desalination: A state-of-the-art review. Desalination, 459, 59-104. doi:10.1016/j.desal.2019.02.008

Radaei, E., Liu, X., Tng, K. H., Wang, Y., Trujillo, F. J., & Leslie, G. (2018). Insights on pulsed bubble control of membrane fouling: Effect of bubble size and frequency. Journal of Membrane science, 554, 59-70. doi:https://doi.org/10.1016/j.memsci.2018.02.058

Radu, A. I., Vrouwenvelder, J. S., van Loosdrecht, M. C. M., & Picioreanu, C. (2010). Modeling the effect of biofilm formation on reverse osmosis performance: Flux, feed channel pressure drop and solute passage. Journal of Membrane science, 365(1), 1-15. doi:https://doi.org/10.1016/j.memsci.2010.07.036

Rahimi, M., Madaeni, S. S., Abolhasani, M., & Alsairafi, A. A. (2009). CFD and experimental studies of fouling of a microfiltration membrane. Chemical Engineering and Processing: Process Intensification, 48(9), 1405-1413. doi:10.1016/j.cep.2009.07.008

Rajaratnam, N. (1976). Turbulent jets: Elsevier.

Ratkovich, N., Chan, C. C. V., Berube, P. R., & Nopens, I. (2009). Experimental study and CFD modelling of a two-phase slug flow for an airlift tubular membrane. Chemical Engineering Science, 64(16), 3576-3584. doi:https://doi.org/10.1016/j.ces.2009.04.048

Ratnayake, P., Setiawan, R., Bao, J., Fimbres-Weihs, G. A., & Wiley, D. E. (2016). Spatio-temporal frequency response analysis of forced slip velocity effect on solute concentration oscillations in a reverse osmosis membrane channel. Computers & Chemical Engineering, 84, 151-161. doi:https://doi.org/10.1016/j.compchemeng.2015.08.016

Rawool, A. S., & Mitra, S. K. (2006). Numerical simulation of electroosmotic effect in serpentine channels. Microfluidics and Nanofluidics, 2(3), 261-269. doi:10.1007/s10404-005-0076-1

Ren, L., Sinton, D., & Li, D. (2003). Numerical simulation of microfluidic injection processes in crossing microchannels. Journal of Micromechanics and Microengineering, 13(5), 739-747. doi:10.1088/0960-1317/13/5/329

Roache, P. J. (1997). Quantification of uncertainty in computational fluid dynamics. Annual review of fluid Mechanics, 29(1), 123-160. doi:https://doi.org/10.1146/annurev.fluid.29.1.123

Rodrigues, C., Garcia-Algado, P., Semião, V., de Pinho, M. N., & Geraldes, V. (2013). Concentration boundary layer visualization in nanofiltration by holographic interferometry with light deflection correction. Journal of Membrane science, 447, 306-314. doi:https://doi.org/10.1016/j.memsci.2013.07.035

Russel, W. B., Russel, W., Saville, D. A., & Schowalter, W. R. (1991). Colloidal dispersions: Cambridge university press.

Salehi, M.-S., Askarishahi, M., Godini, H. R., Görke, O., & Wozny, G. n. (2016). Sustainable process design for oxidative coupling of methane (OCM): comprehensive reactor engineering via computational fluid dynamics (CFD) analysis of OCM packed-bed membrane reactors. Industrial & Engineering Chemistry Research, 55(12), 3287-3299. doi:https://doi.org/10.1021/acs.iecr.5b03292

Santiago, J. G. (2001). Electroosmotic Flows in Microchannels with Finite Inertial and Pressure Forces. Analytical Chemistry, 73(10), 2353-2365. doi:10.1021/ac0101398

Schwinge, J., Wiley, D. E., & Fletcher, D. F. (2002a). A CFD study of unsteady flow in narrow spacer-filled channels for spiral-wound membrane modules. Desalination, 146(1), 195-201. doi:https://doi.org/10.1016/S0011-9164(02)00470-8

Schwinge, J., Wiley, D. E., & Fletcher, D. F. (2002b). Simulation of the Flow around Spacer Filaments between Channel Walls. 2. Mass-Transfer Enhancement. Industrial & Engineering Chemistry Research, 41(19), 4879-4888. doi:10.1021/ie011015o

Scott, K. (1995). Handbook of industrial membranes: Elsevier.

Snel, H. (2003). Review of aerodynamics for wind turbines. Wind Energy: An International Journal for Progress and Applications in Wind Power Conversion Technology, 6(3), 203-211. doi:https://doi.org/10.1002/WE.97

Sparks, T., & Chase, G. (2016). Section 2 - Filter Media. In T. Sparks & G. Chase (Eds.), Filters and Filtration Handbook (Sixth Edition) (pp. 55-115). Oxford: Butterworth-Heinemann.

Spiegler, K. S., & Macleish, J. H. (1981). Molecular (osmotic and electro-osmotic) backwash of cellulose acetate hyperfiltration membranes. Journal of Membrane science, 8(2), 173-192. doi:https://doi.org/10.1016/S0376-7388(00)82089-X

Steinhauser, M. O. (2017). Computational multiscale modeling of fluids and solids: Springer.

Streeter, V., Wylie, E., & Bedford, K. (1985). Fluid Mechanics (8th ed.): McGraw-Hill.

Su, X., Li, W., Palazzolo, A., & Ahmed, S. (2018). Concentration polarization and permeate flux variation in a vibration enhanced reverse osmosis membrane module. Desalination, 433, 75-88. doi:https://doi.org/10.1016/j.desal.2018.01.001

Su, X., Li, W., Palazzolo, A., & Ahmed, S. (2019). Permeate flux increase by colloidal fouling control in a vibration enhanced reverse osmosis membrane desalination system. Desalination, 453, 22-36. doi:https://doi.org/10.1016/j.desal.2018.12.003

Sun, B., Ahmed, A., Atkinson, C., & Soria, J. (2020). A novel 4D digital holographic PIV/PTV (4D-DHPIV/PTV) methodology using iterative predictive inverse reconstruction. Measurement Science and Technology, 31(10), 104002. doi:10.1088/1361-6501/ab8ee8

Taha, T., Cheong, W. L., Field, R. W., & Cui, Z. F. (2006). Gas-sparged ultrafiltration using horizontal and inclined tubular membranes—A CFD study. Journal of Membrane science, 279(1), 487-494. doi:https://doi.org/10.1016/j.memsci.2005.12.063

Taha, T., & Cui, Z. F. (2002). CFD modelling of gas-sparged ultrafiltration in tubular membranes. Journal of Membrane science, 210(1), 13-27. doi:https://doi.org/10.1016/S0376-7388(02)00360-5

Taha, T., & Cui, Z. F. (2006a). CFD modelling of slug flow in vertical tubes. Chemical Engineering Science, 61(2), 676-687. doi:https://doi.org/10.1016/j.ces.2005.07.022

Taha, T., & Cui, Z. F. (2006b). CFD modelling of slug flow inside square capillaries. Chemical Engineering Science, 61(2), 665-675. doi:https://doi.org/10.1016/j.ces.2005.07.023

Taheri, A. H., Sim, L. N., Chong, T. H., Krantz, W. B., & Fane, A. G. (2015). Prediction of reverse osmosis fouling using the feed fouling monitor and salt tracer response technique. Journal of Membrane science, 475, 433-444. doi:10.1016/j.memsci.2014.10.043

Toh, K., Liang, Y., Lau, W., & Weihs, G. F. (2020a). The techno-economic case for coupling advanced spacers to high-permeance RO membranes for desalination. Desalination, 491, 114534. doi:https://doi.org/10.1016/j.desal.2020.114534

Toh, K. Y., Liang, Y. Y., Lau, W. J., & Fimbres Weihs, G. A. (2020b). A review of CFD modelling and performance metrics for osmotic membrane processes. Membranes, 10(10), 285. doi:https://doi.org/10.3390/membranes10100285

Unal, B. O. (2022). Membrane autopsy study to characterize fouling type of RO membrane used in an industrial zone wastewater reuse plant. Desalination, 529, 115648.

Versteeg, H. K., & Malalasekera, W. (2007). An introduction to computational fluid dynamics: the finite volume method: Pearson education.

Vinuesa, R., & Brunton, S. L. (2022). Enhancing computational fluid dynamics with machine learning. Nature Computational Science, 2(6), 358-366. doi:https://doi.org/10.1038/s43588-022-00264-7

Vrouwenvelder, J. S., Picioreanu, C., Kruithof, J. C., & van Loosdrecht, M. C. M. (2010). Biofouling in spiral wound membrane systems: Three-dimensional CFD model based evaluation of experimental data. Journal of Membrane science, 346(1), 71-85. doi:10.1016/j.memsci.2009.09.025

Wardeh, S., & Morvan, H. P. (2008). CFD simulations of flow and concentration polarization in spacer-filled channels for application to water desalination. Chemical Engineering Research and Design, 86(10), 1107-1116. doi:https://doi.org/10.1016/j.cherd.2008.04.010

Wiley, D. E., & Fletcher, D. F. (2003). Techniques for computational fluid dynamics modelling of flow in membrane channels. Journal of Membrane science, 211(1), 127-137. doi:https://doi.org/10.1016/s0376-7388(02)00412-x

Xue, Y. L., Zhang, R., Cao, B., & Li, P. (2021). Chapter 20 - Tubular membranes and modules. In T.-S. Chung & Y. Feng (Eds.), Hollow Fiber Membranes (pp. 431-448): Elsevier.

Zare, M., Zokaee Ashtiani, F., & Fouladitajar, A. (2013). CFD modeling and simulation of concentration polarization in microfiltration of oil–water emulsions; Application of an Eulerian multiphase model. Desalination, 324, 37-47. doi:https://doi.org/10.1016/j.desal.2013.05.022

Zhang, J.-b., He, G.-w., & Liu, F. (2006). Electro-osmotic flow and mixing in heterogeneous microchannels. Physical Review E, 73(5), 056305. doi:10.1103/PhysRevE.73.056305